https://doi.org/10.1016/j.jobe.2020.101815

Wind characteristics atop Shanghai Tower during typhoon Jongdari using field monitoring data

Jie Wu[a], Ningtao Hu[a], You Dong[b], Qilin Zhang[a], Bin Yang[a]

[a] *College of Civil Engineering, Tongji University, 1239 Siping Road, Shanghai 200092, PR China*

[b] *Department of Civil and Environmental Engineering, The Hong Kong Polytechnic University, Hong Kong, PR China*

Abstract: In this paper, detailed analysis of the field wind data atop the Shanghai Tower is conducted to investigate the wind characteristics evolution generated by typhoon Jongdari, which could provide useful information for the high altitude wind features in dense building landform and aid the wind-resistant design of 600 m+ super-tall buildings. The necessity of data preprocessing is discussed and some precautions for processing the wind directions are pointed out. The correlations of the mean wind speeds in different averaging times are analyzed using a non-stationary wind velocity model. The fluctuation wind characteristics at evolutional stages of the typhoon including turbulence intensity, gust factor, integral scale of turbulence and power spectrum are discussed and compared with several typhoons measured atop the other super-tall buildings. Based on the analysis, the ratio of the mean wind speeds between 10 min and 1 h averaging times remains stable. It is found that there is a slight difference between the linear and nonlinear fitting of three longitudinal parameters, i.e. the gust factor, turbulence intensity and gust duration time, but obvious error exists as to the linear fitting of the lateral parameters. The statistical results of the turbulent integral scale reflect relatively violent excitation of the turbulent wind to the structure and the spectra of turbulent velocity are associated with various characteristics in different stages of the typhoon.

Key words: wind characteristics; field monitoring; typhoon; super-tall building; Shanghai Tower

1. Introduction

In recent years, increasing demands for residential space have led to a large number of high-rise buildings especially in some coastal areas, where are often vulnerable to strong winds. Therefore, wind characteristics and typhoon evolution are of great significance for wind-resistance design and disaster prevention of these high-rise buildings. Due to the particularity of structure and mechanism of typhoons and the influence of bluff body flow around high-density buildings, it is difficult for wind tunnel to simulate complex wind characteristics in high-rise building groups. Therefore, field monitoring becomes the most direct and reliable means to investigate the characteristics. These measurements have supplied people with real wind loads which have inherently included full complexity [1]. In the past few decades, researches in different countries have established the relevant wind databases by measurements, such as Norway's Froya database [2], Canada's and Britain's near sea wind observation database [3], etc.

Wind data are often monitored from wind observation towers in the field of meteorology. By monitoring at four heights of a 40-m tower, Wang et al. [4,5] investigated turbulence characteristics including wind-speed profiles, turbulence integral scales, power spectra, correlations, and coherences during typhoon Meari and Muifa (2011). Based on the field monitoring on a 100-m high tower, Li et al. [6] investigated wind characteristics of typhoon Hagupit (2008), and the relevant results were compared with that of typhoon Maemi (2003) and other three hurricanes. Song et al. [7] investigated Typhoon Hagupit (2008) in the marine surface boundary layer by observing from a 100-m high offshore meteorological tower. However, the wind towers are usually built on flat and wide terrain, that is different from urban complex one, the relevant measurements of wind characteristics associated with typhoons for super-tall buildings are relatively scarce, especially in dense building landform.

In the past decades, with the development of information technology and sensors, many super-tall buildings have been equipped with structural health monitoring (SHM) systems [8-12], which enabled people to monitor the environmental wind continuously atop building for a long time, obtaining the

valuable first-hand data. Guangdong-Hong Kong-Macao Greater Bay Area (BGA) always suffers from several typhoons every year, and it provides excellent opportunities to study the characteristics of typhoons in urban. Li et al. [13-16] analyzed the measured wind data atop numbers of super-tall buildings in BGA, such as Ping An International Finance Centre (592.5 m) in Shenzhen, the International Finance Centre (420 m) in Hong Kong, and CITIC Plaza Tower (391 m) in Guangzhou, including the characteristics of high-altitude wind field, wind load distribution and wind-induced response of the structure. Wang et al. [17] investigated the pulsating characteristics of three adjacent high-rise buildings under typhoon Moranti (2016).

Previous studies (e.g. Li et al. [14], Powell et al. [18]) indicated that the surface winds of a landfall tropical cyclone (TC) may be significantly affected by local topography. Shanghai, where several super-tall and many tall buildings were built in the past three decades, experiences fewer typhoons than BGA and the corresponding researches on measured data become particularly valuable. Based on the measured wind data atop Shanghai World Financial Center (492 m), An et al. [19] investigated the characteristics of typhoon Muifa (2011), Quan et al. [20] investigated the normal wind characteristics, and Huang and Gu [21] studied wind characteristics for typhoon Chan-hom (2015). Wu et al. [22] analyzed normal wind characteristics from the measured data atop the Shanghai Tower. In addition, the wind induced vibration of super-tall buildings has been widely investigated by the full-scale measurements and wind tunnel tests [23-25]. Au et.al [26] presented observations on the identified modal properties of two tall buildings using ambient vibration data collected during strong wind events. Zhang et al. [27] utilized the fast Bayesian method to analyze the ambient vibration data of the Shanghai Tower at different construction stages and identified the dynamic parameters of the structure. Fu et al. [28] evaluated the dynamic characteristics and wind effects on the Guangzhou West Tower. Although many measurements and theoretical researches on the wind characteristics and wind induced vibration under typhoon have been conducted, the studies on the high-altitude of the 600 m+ super-tall building are still scarce.

In this paper, the wind speeds and directions atop the Shanghai Tower under the influence of typhoon Jongdari are monitored and recorded. These data are preprocessed firstly to reduce the influence of outlier data and noise. In particular, some precautions for processing the wind directions are pointed out and a solution is put forward. Based on a non-stationary calculation model, the differences of mean wind in various average time are analyzed. In order to investigate the wind characteristics evolution under the investigated typhoon, the fluctuation wind characteristics at different stages are presented and discussed, such as turbulence intensity, gust factor, integral scale of turbulence and power spectrum. These analysis results are also compared with several typhoons measured atop other super-tall buildings. The relevant conclusions could provide useful information for the high altitude wind features in dense building landform and wind-resistant design of 600 m+ super-tall buildings.

2. Typhoon Jongdari and field measurement profile

Jongdari developed as a tropical depression in the northeast of the Pacific Ocean on July 25, 2018, and made landfall over Jinshan coast, Shanghai, at about 10:30 on August 3 as a tropical storm with the maximum wind force of 9th grade (in Beaufort Scale, 23 m / s) near its center and the minimum central pressure of 985 hPa. Later, it continued to move along the northwest direction and weakened gradually into the tropical depression. At 23:00 the wind-rain intensity decreased and National Meteorological Center of CMA (China) stopped numbering it.

(a) (b)

Fig. 1. Path of typhoon Jongdari. (a) Typhoon center track; (b) Shanghai tower

The Shanghai Tower, located in Lujiazui, Shanghai, China, is the second tallest building in the world with a height of 632 m. It consists of a 121-story main building, a 5-story podium building, and a 5-story basement. As shown in Fig 1 (b), it is surrounded by several super-tall and many tall buildings, which belongs to a typical rough underlying surface of urban, making the wind field characteristics complex. As shown in Fig. 2, an ultrasonic anemometer with an acquisition sampling rate (ASR) of 100Hz is installed atop the building. The specific parameters of the anemometer are listed in Table 1.

Table 1. Specific parameters of ultrasonic anemometer

Wind speed parameter	Technical index	Wind direction parameter	Technical index
Range	0 ~ 40m	Range of wind direction	0.0 ~ 359.9º
Resolving power	0.1 m/s	Range of angle	± 60 º
Threshold	0.01 m/s	Resolving power	0.1 º
Precision	±1% rms ± 0.05 m/s	Precision	± 2 º(1 ~ 30 m/s)

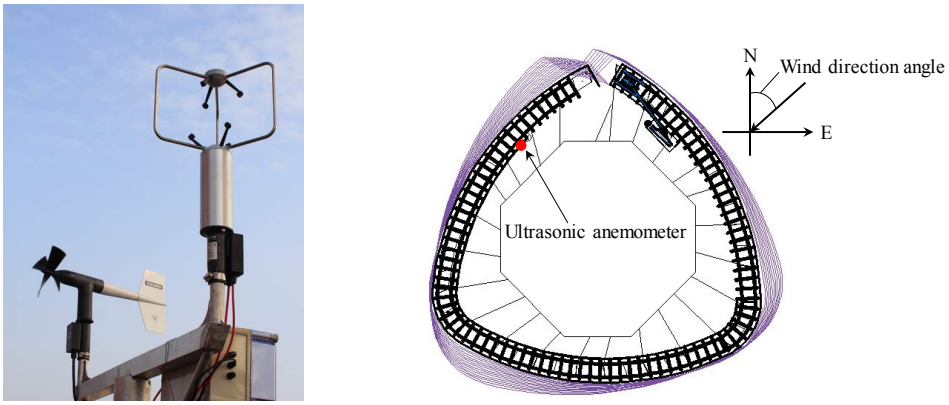

Fig. 2. Ultrasonic anemometer and its installation location

3. Data preprocessing

The data from 7:00 to 14:00 on August 3, 2018, were used to analyze the basic characteristics of the typhoon. Since the ultrasonic anemometer determines the airflow velocity by time difference along ultrasonic propagation path, any substances obstructing the path would reduce its accuracy, resulting in outlier data (or abnormal value). For the purpose of judging and eliminating these outliers, a method, which combined with a moving window and threshold of 3 times standard deviation, is used to preprocess the data. Meanwhile, the sensor is inevitably suffered from external interference during its work, hence it is necessary to denoise the signal (or data). In general, denoise methods include commonly filter technologies, Kalman filtering, empirical mode decomposition (EMD) and wavelet denoising. In this paper, a wavelet hard-threshold denoising method is utilized by adopting Sym4

wavelet. Sym4 wavelet is orthogonal and compactly supported, which can reduce a certain phase distortion of signal decomposition and reconstruction.

It should be paid special attention in dealing with the data of wind directions. When the two wind directions of adjacent time are in A and B respectively as shown in Fig.3, there are two possibilities for the change routes: ② and ①, which, obviously, is more likely. If the above-mentioned preprocessing is directly applied for the data of wind directions, it is very possible to change along route ②. Therefore, a "continuity conversion" is carried out before the preprocessing being applied. The wind direction at the time i is denoted by $\alpha(i)$, and the "continuity conversion" goes as follows:

(1) If $\alpha(i) \geqslant 360^{o} - \beta$ and $\alpha(i+1) \leqslant \beta$, then $\alpha(i+1) = \alpha(i+1) + 360^{o}$; and

(2) If $\alpha(i) \leqslant \beta$ and $\alpha(i+1) \geqslant 360^{o} - \beta$, then $\alpha(i+1) = \alpha(i+1) - 360^{o}$.

where β needs to be assigned and equals 90^{o} herein. In this way, the range of the data changes to $[-\beta, 360° + \beta]$. After the "continuity conversion" and the outlier data being removed as well as denoise, the converted data need to be restored to original range, i.e., $\alpha(i) = \alpha(i) - 360^{o}$ for $\alpha(i) > 360^{o}$, and $\alpha(i) = \alpha(i) + 360^{o}$ for $\alpha(i) < 0^{o}$.

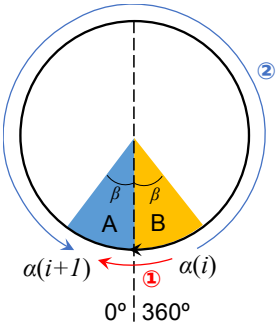

Fig. 3. Diagram for discontinuity of wind speeds

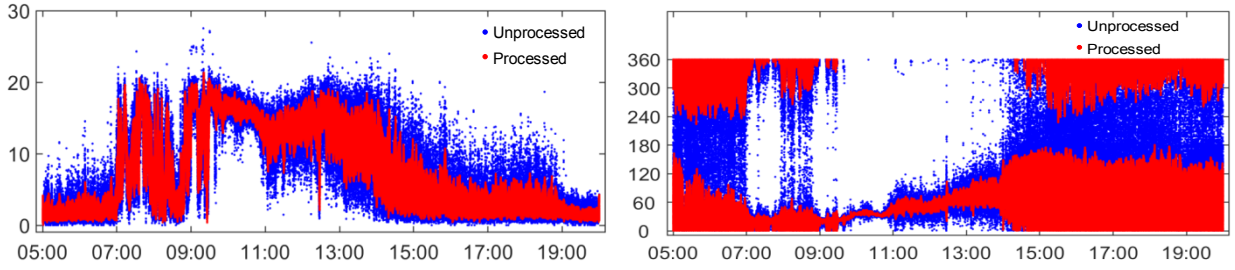

(a) (b)

Fig. 4. Unprocessed and processed (a) wind speeds; and (b) wind directions

Fig. 4 shows the comparison of wind data before and after preprocessing (including outlier data processing and wavelet hard-threshold denoising). It can be seen that the above processing methods can remove the abnormal value effectively without altering the signal features. As shown in Fig. 4 (a), the wind speeds were relatively high from 7:30 to 8:00 but became low with violent fluctuation of wind directions from 8:20 to 8:50, and then increased sharply until tended to be stable after 8:55. The measured instantaneous maximum wind speed occurred between 8:50 and 9:10, reaching at 25.8 m/s.

4. Analysis of wind characteristics

Structural wind engineering mainly focuses on the wind characteristics of the atmospheric boundary layer, consisting of the averaging and fluctuation components. In this paper, the characteristics of the typhoon Jongdari are analyzed based on a non-stationary wind velocity model, including mean wind speed and direction, turbulence intensity, gust factor, integral scale of turbulence, and the spectra of turbulent velocity.

4.1 Mean wind speed and direction

For traditional analysis method, wind velocity is regarded hypothetically as a stationary random process and can be divided into constant component and fluctuating one, which stands for a stationary wind velocity model. This is reasonable for normal wind on open terrain. However, the wind velocity of typhoon, as a strong cyclonic airflow, is a non-stationary process. Therefore, the mean wind speeds are calculated combined with a moving window in time to establish a non-stationary wind velocity model. This model can diminish the deviation of wind characteristics due to different ways of segmentation sections in the stationary one. Each moving time step is assigned by 1 min, so one point can be obtained per minute. The model is described as follows.

In three-dimensional airflow, the wind velocity vector in the horizontal direction can be decomposed into two perpendicular components of X and Y directions. Wind speed at the time i is denoted by $V(i)$ and the incoming wind direction angle is denoted by $\alpha(i)$. To obtain the mean wind speeds and directions, a Cartesian coordinate system is established firstly to decompose the wind velocity into X and Y components:

$$u_x(i) = V(i)\cos\alpha(i) \tag{1}$$

$$u_y(i) = V(i)\sin\alpha(i) \tag{2}$$

$$\overline{u}_x(k) = \frac{1}{N_s}\sum_{i=1}^{N}\Omega(i-k)u_x(i) \tag{3}$$

$$\overline{u}_y(k) = \frac{1}{N_s}\sum_{i=1}^{N}\Omega(i-k)u_y(i) \tag{4}$$

where $\overline{u}_x$ and $\overline{u}_y$ = mean wind speeds in X and Y directions at the time k, respectively, N = the number of data points, and $\Omega(\bullet)$ represents rectangular window function:

$$\Omega(i) = \begin{cases} 1, & i \in [-\frac{N_s}{2}, \frac{N_s}{2}] \\ 0, & \text{else} \end{cases} \tag{5}$$

where N_s = the width of rectangular window. The mean wind speed denoted by $U(k)$ and the mean wind direction angle denoted by $D(k)$ can be calculated as follows:

$$U(k) = \sqrt{\overline{u}_x^2(k) + \overline{u}_y^2(k)} \tag{6}$$

$$D(k) = \begin{cases} \arctan\left(\dfrac{\overline{u}_x(k)}{\overline{u}_y(k)}\right) + H(-\overline{u}_x(k))\times 180°, & \overline{u}_y(k) \neq 0 \\ 90° + H(-\overline{u}_x(k))\times 180°, & \overline{u}_y(k) = 0 \end{cases} \tag{7}$$

if D < 0, then D = D + 360° , where $H(\bullet)$ is Heaviside step function:

$$H(i) = \begin{cases} 1, & i \geq 0 \\ 0, & \text{else} \end{cases} \tag{8}$$

The longitudinal fluctuating wind speed denoted $u(i)$ and the lateral one denoted $v(i)$ are respectively:

$$u(i) = u_x(i)\sin D(k) + u_y(i)\cos D(k) - U(k) \tag{9}$$

$$v(i) = -u_x(i)\cos D(k) + u_y(i)\sin D(k) \tag{10}$$

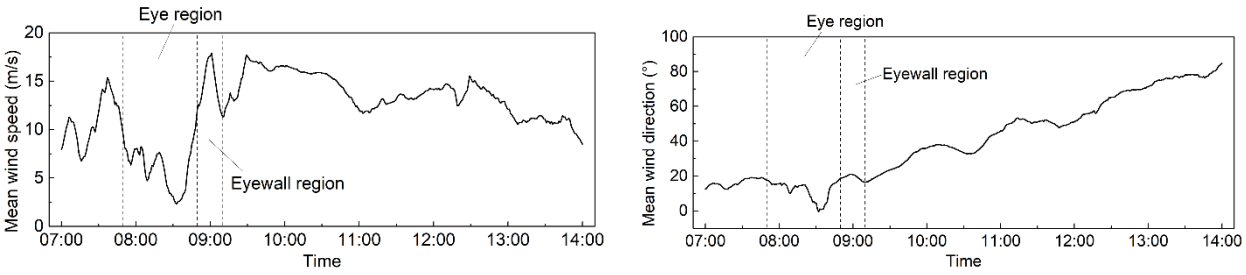

(a) (b)

Fig. 5. Time history of 10 min mean (a) wind speeds; and (b) wind directions

Fig.5 plots the time history of the 10 min mean wind speeds and directions. From 7:50 to 8:50 the mean wind speeds decreased obviously, which means that the typhoon eye was passing by. The maximum mean wind speed before the coming of typhoon eye reached 15.4 m/s, with the wind direction about 21°. After the eye, the mean wind directions changed from 20° to 80° gradually. From 8:55 to 9:08, the eyewall came when the mean wind speeds reached the maximum value of 17.9 m/s and the wind speeds became weakening slightly after 10:30.

The duration time of mean wind speed varies among different countries. For example, 3 s is adopted in Britain and Australia, 1 h in Canada, 10 min in China and Denmark, but the instantaneous maximum wind speed is used in Japan. Herein, for the investigated case, the mean wind speeds are volatile and high within 3 s average time (Fig. 6 (a)), but they are relatively stable and small within 10 min and 1 hour average time (Fig. 6 (b)).The detailed results are shown in Fig. 6.

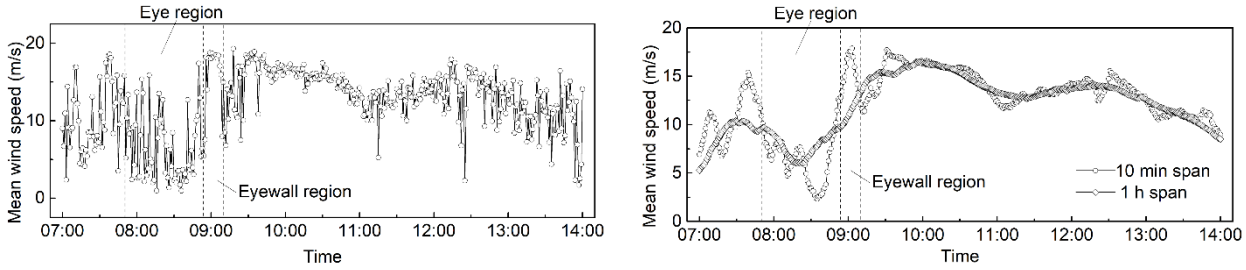

(a) (b)

Fig. 6. Mean wind speeds within time of (a) 3 s; and (b) 10 min and 1 h

To assess the correlation of the mean wind speeds within various averaging times, the linear fitting with zero intercept is carried out, and the results are indicated in Fig. 7. The Pearson coefficient of mean wind speeds between 1 hour and 10 min is 0.989, and that between 3 s and 10 min is 0.979, both of which indicate a linear correlation.

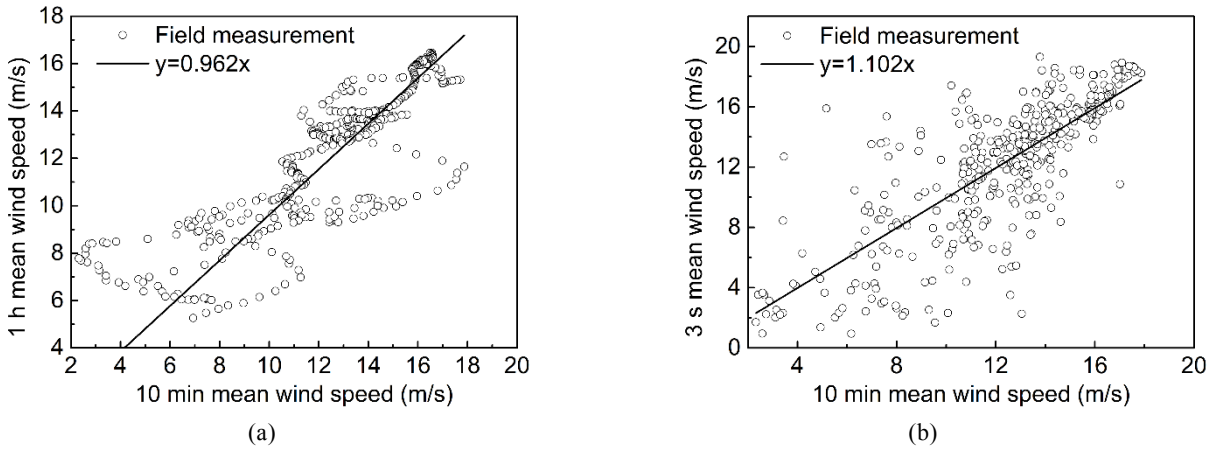

(a) (b)

Fig. 7. Correlation of the mean wind speeds within (a) 1 h and 10 min; and (b) 3 s and 10 min

The correlations of the mean wind speeds within various averaging times are compared with those of Ref. [21], as listed in Table 2. The correlation of 1 hour to 10 min in this paper is similar to that in Ref. [21], whereas that of 3 s to 10 min has a deviation of -8.6%. It indicates that 3 s is not a suitable averaging time due to its instability. However, the mean wind speeds within both 10 min and 1 hour reflect the main change of wind speeds well. Considering a larger amount of data required for 1 hour, 10 min could be selected for the computational process of wind speed.

Table 2. Correlations of average wind speeds within different duration time periods

Correlations	Ref. [21]	This paper	Deviation
$\overline{v}_{1h}$:$\overline{v}_{10min}$	0.953:1	0.962:1	0.94%
$\overline{v}_{3s}$:$\overline{v}_{10min}$	1.206:1	1.102:1	-8.6%

4.2 Characteristics of fluctuating wind

Fluctuating components of flow play an important role in the dynamics of the structure especially for tall buildings [29]. Flexible structures may exhibit resonant amplification effects and the aerodynamic behavior of structures may depend strongly upon the turbulence in the airflow. The features of the atmospheric turbulence include customarily turbulence intensity, gust factor, integral scale of turbulence, the spectra of turbulent velocity fluctuations, etc.

4.2.1 Turbulence intensity

Turbulence intensity describes the relative intensity of fluctuating wind and can be determined by the following equation:

$$I_i = \frac{\sigma_i}{U}, i = u, v \tag{11}$$

where σ_i = root mean square (RMS) of the fluctuating component in direction i, u denotes longitudinal direction, and v denotes lateral one.

The 10 min duration time is adopted to calculate the turbulence intensities herein, the time history of which is plotted in Fig. 8. It can be seen that the turbulence intensities perform obvious evolutions during different stages, including successively eye region, eyewall region, and outskirt regions. For the convenience of description, the period of 9:30-12:10 is denoted by outskirt region I and that of 12:10-14:00 is denoted by outskirt region II. Turbulence intensity of each stage of typhoon Jongdari is compared with that of typhoon Muifa [19], Chan-hom [21] in Shanghai, Imbudo [13] in Shenzhen, and the normal wind [30] measured atop the Shanghai World Financial Center, as listed in Table 3.

As shown in Fig. 8 and Table 3, the longitudinal turbulence intensities are greater than the lateral ones. In outskirt region I, the turbulence intensities are relatively stable but leap at about 11:00, which may be attributed to the change of wind directions (see Fig. 5 (a)) and be influenced by the obstructing of surrounding buildings. In this region, both longitudinal and lateral turbulence intensities are small, close to that of typhoon Chan-hom [21]. In outskirt region II, both longitudinal and lateral turbulence intensities increase. Longitudinal turbulence intensities are close to those of eyewall region, but the lateral ones are significantly different. In eye region, turbulence intensities increase due to low wind speeds. In eyewall region, the turbulence intensities reduce to a minimum of 0.0865, which is close to the normal wind [30].

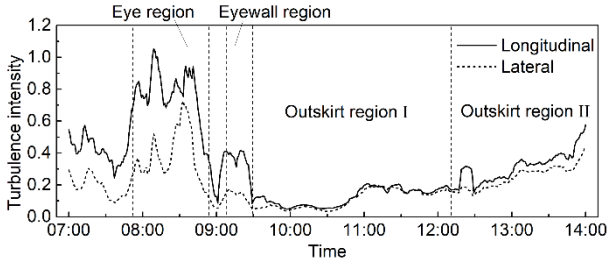

Fig. 8. Time history of turbulence intensity

Table 3. Comparison of turbulence intensities

Measured data	Measured height (m)	Mean of I_u	Range of I_u	Mean of I_v	Range of I_v	I_u:I_v
Outskirt region I	632	0.0968	0.0485~0.209	0.0774	0.0335~0.192	1:0.800
Outskirt region II	632	0.263	0.145~0.577	0.219	0.132~0.436	1:0.833
Eyewall region	632	0.26	0.0865~0.413	0.0896	0.0523~0.153	1:0.345
Eye region	632	0.815	0.596~1.054	0.421	0.212~0.725	1:0.517
Typhoons Muifa [19]	494	0.14	0.05~0.29	0.13	0.04~0.26	1:0.929
Typhoon Chan-hom [21]	494	0.107	0.061~0.155	0.066	0.040~0.158	1:0.617
Typhoon Imbudo [13]	345	0.196	-	0.112	-	1:0.571
Normal wind [30]	436	0.201	-	0.066	-	1:0.328

Figs. 9 (a) and 9 (b) show the variation of turbulence intensities with mean wind speeds. The Pearson coefficient between longitudinal turbulence intensities and average wind speeds is - 0.879 and that of lateral one is - 0.929, both of which are close to -1, indicating negative linear correlation: I_u = - 0.879 U + 0.771, I_v = -0.044 U + 0.761. Fig.9 (c) shows the correlation between longitudinal and lateral turbulence intensities from 10:00 to 13:50, while wind speed is relatively stable. Their Pearson coefficient is 0.993. According to linear fitting without intercept, there is a ratio of I_u : I_v = 1 : 0.835, which is close to that for both in outskirt regions I and II. Meanwhile, it is closest to that of typhoon Muifa [19] shown in Table 3, but quite different from that of typhoon Chan-hom [21] and Imbudo [13], which may due to the fact that these ratios were calculated by the measured data in the whole typhoon duration. In fact, it is unreasonable to use one value to represent the characteristics of turbulence intensities during the whole process of typhoon while the wind characteristics change greatly. Therefore, the data should be selected during the process when the wind characteristics are relatively stable. In this way, the computed turbulence intensities can describe the wind characteristics of the corresponding period accurately.

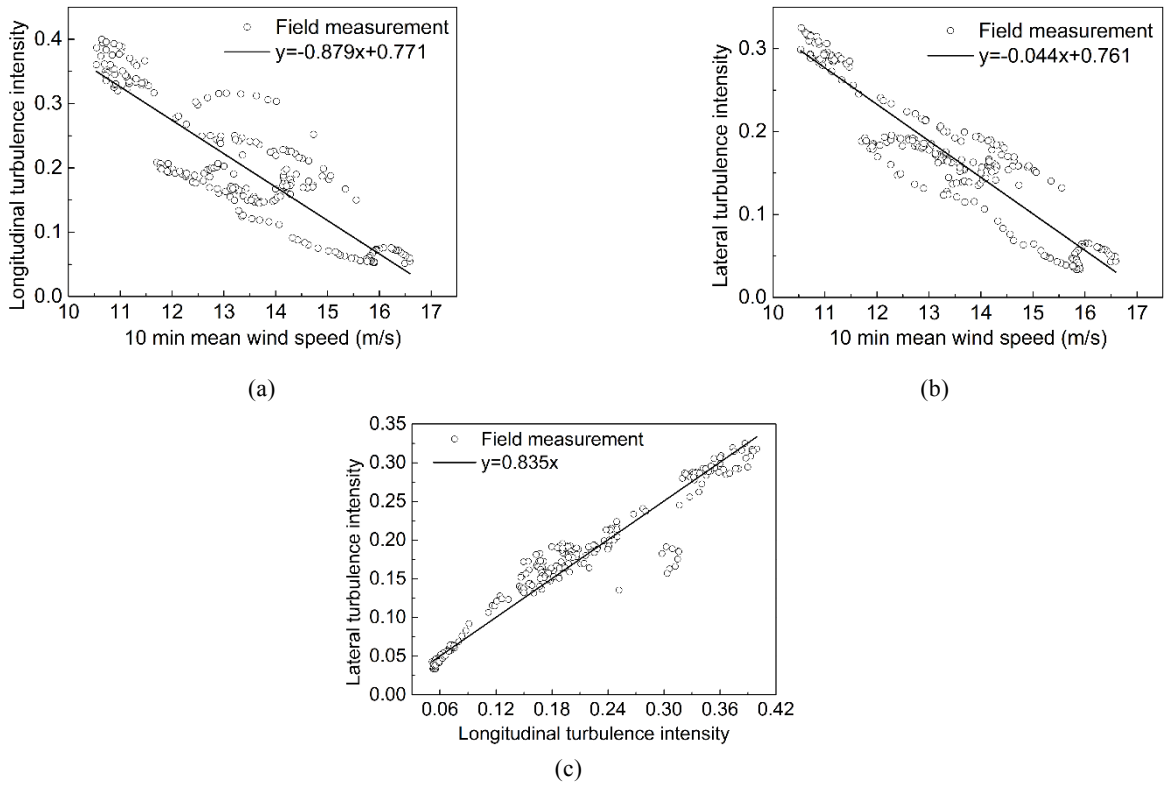

Fig. 9. Variations of (a) longitudinal turbulence intensities with mean wind speeds; (b) lateral turbulence intensities with mean wind speeds; and (c) lateral turbulence intensities with the longitudinal one

4.2.2 Gust factor

To consider the influence of gusting wind, the mean wind pressure or mean wind pressure coefficient is often used to predict the peak pressure on the surface of some cladding and enclosure structures, hence the gust factor should be calculated. Gust factor is defined as the ratio of the peak gust speed over a short duration t_g to the mean wind speed U in a relatively longer duration T.

Longitudinal gust factor:

$$G_u(t_g,T)=\frac{U(T)+u_g(t_g)}{U(T)}=1+\frac{u_g(t_g)}{U(T)} \tag{12}$$

Lateral gust factor:

$$G_v(t_g,T)=\frac{v_g(t_g)}{U(T)} \tag{13}$$

where u_g and v_g = the maxima of longitudinal and lateral mean wind speeds in duration t_g, respectively. In this paper, t_g = 3 s and T = 10 min.

As shown in Fig. 10, the gust factors reached at maximum when the typhoon eye passed through, decreased obviously in the eyewall region, and tended to be relatively stable in outskirt region.

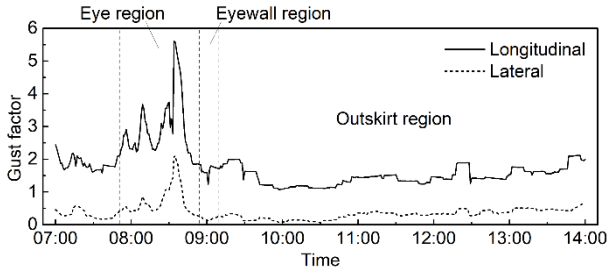

Fig. 10. Time history of gust factors

Herein, gust factors are obtained from the data between 10:00 and 13:50, while the wind characteristics were stable. Fig. 11 shows the linear correlation between the gust factors and the mean wind speeds: G_u = -0.982U + 2.752 with the Pearson coefficient of -0.763, and G_v = -0.0833U + 1.178 with the Pearson coefficient of -0.864.

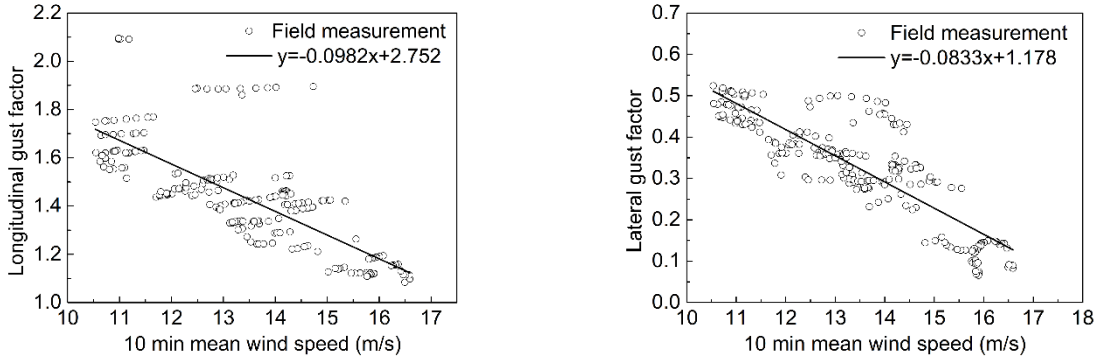

(a) (b)

Fig. 11. Variation of gust factors with mean wind speeds: (a) longitudinal direction; and (b) lateral direction

Ishizaki [31] suggested that the relationship between G_u, I_u, and t_g can be expressed by following equation:

$$G_u(t_g)=1+aI_u^b\ln(\frac{T}{t_g}) \tag{14}$$

where a and b = the parameters to be fitted, T = 10 min. Best fitting with this equation leads to

$G_u(t_g) = 1 + 0.339 I_u^{0.804} \ln(\frac{600}{t_g})$, as shown in Fig. 12.

Ishizaki [31] fitted the equation (14) with duration time of 10 min and 1 h, respectively, and suggested that a = 0.5 and b = 1.0, which means a linear relationship between G_u and I_u for each t_g. Choi [32] fitted the equation with duration time of 1 h and the results were a = 0.63 and b = 1.27, which indicates a nonlinear relationship. Fig. 13 shows the comparison between the results in this paper and those suggested by Ishizaki as well as Choi. The G_u of this paper is larger than that of Choi for I_u<0.278, but smaller than that for I_u > 0.278. However, the G_u of Ishizaki is just between those of this paper and Choi.

Fig. 14 (a) shows the linear and nonlinear fittings of G_u, I_u, and t_g, and Fig. 14 (b) illustrates the deviations between them which are less than 10% overall. Quan et al. [20] compared the linear and nonlinear fittings for T = 10 min, t_g = 3 s with the founding that they are almost similar, which is consistent with the results from this paper. As shown in Fig. 14 (b), when t_g < 2 s, I_u < 0.03 or I_u > 0.4, the gust factors of nonlinear fitting are 5% smaller than those of linear fitting. For t_g > 3 s or t_g = 3 s, which is commonly used, the gust factors of nonlinear fitting are greater than those of linear fitting, which means a safer condition to bearing capacity design of the enclosure structures.

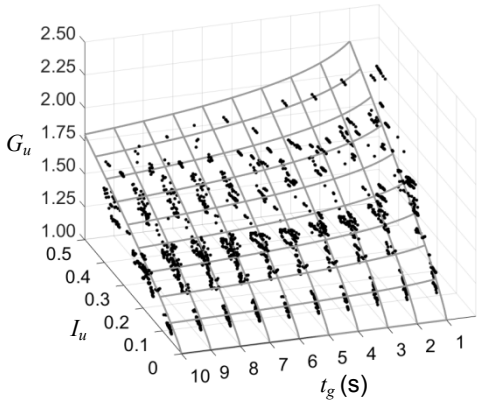

Fig. 12. Variation of longitudinal gust factors with turbulence intensities and gust duration time

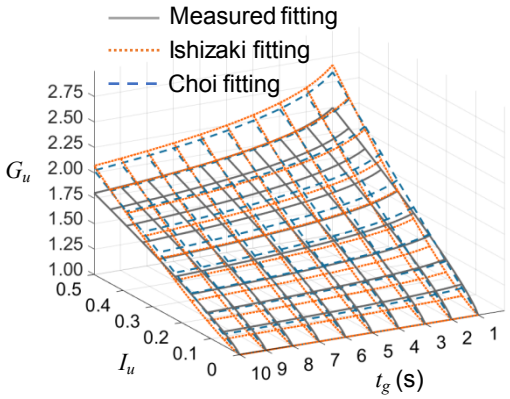

Fig. 13. Comparison of fitting results

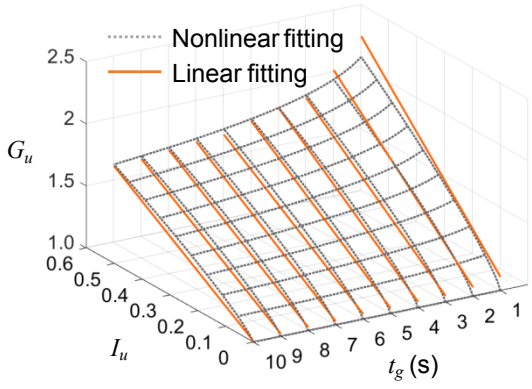

(a)

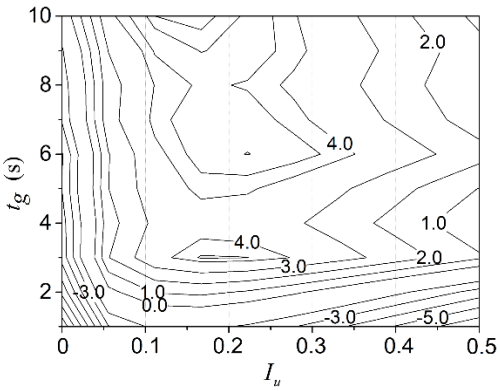

(b)

Fig. 14. Linear and nonlinear fitting of longitudinal gust factors with turbulence intensities and gust duration time: (a) comparison; and (b) deviation (%)

Similar with the definitions format of equation (14), relationship for G_v, I_v, and t_v can be defined as follows:

$$G_v(t_g) = cI_v^d \ln(\frac{600}{t_g}) \tag{15}$$

where c and d = parameters to be fitted. Fig. 15 shows the best fitting in this paper, with the result of

$$G_v(t_g) = 0.210 I_v^{0.656} \ln(\frac{600}{t_g}).$$

Both linear and nonlinear fittings are shown in Fig. 16 (a), and the deviations between them are illustrated in Fig. 16 (b). For $I_v > 0.25$, the gust factors of nonlinear fitting are much smaller than those of linear fitting. When $I_v < 0.25$ and $t_g \geq 3$ s, the gust factors of nonlinear fitting are larger than those of linear fitting with the maximum deviation of more than 80%. Therefore, the values of lateral gust factors may be smaller if they are converted from the turbulence intensities by linear fitting.

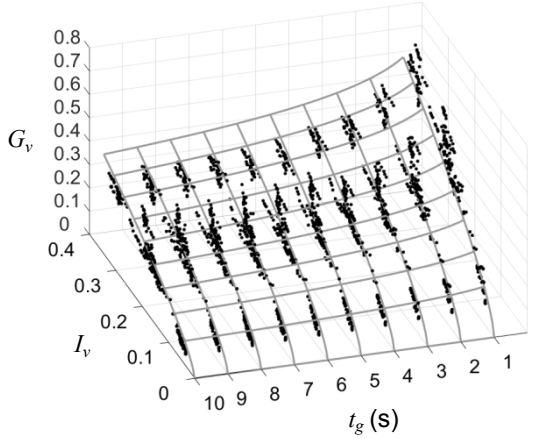

Fig. 15. Variation of lateral gust factors with turbulence intensities and gust duration time

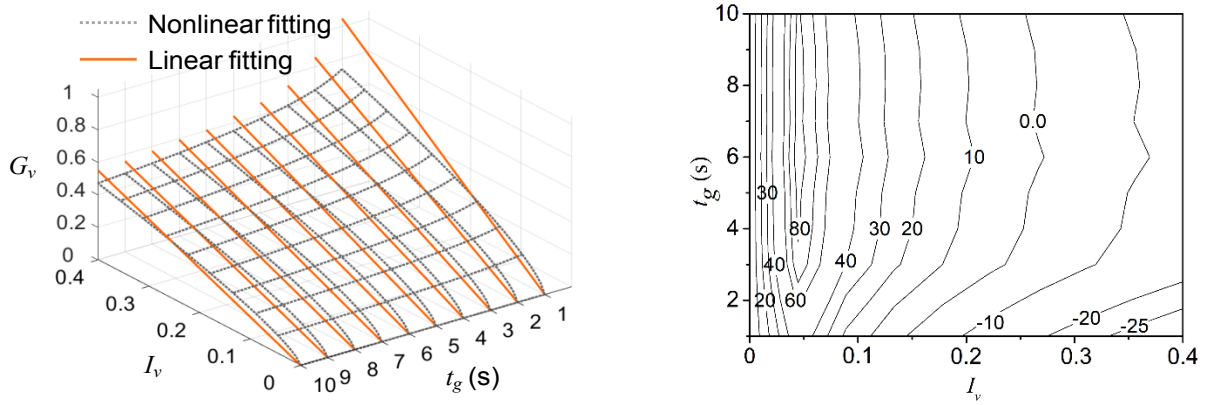

(a) (b)

Fig. 16. Linear and nonlinear fitting of lateral gust factors with turbulence intensities and gust duration time: (a) comparison; and (b) deviation (%)

4.2.3 Integral scale of turbulence

The velocity fluctuations of airflow passing a point would be caused by a superposition of eddies transported by the mean wind. Integral scale of turbulence can measure the average size of the turbulent eddies of the airflow. There are three vortex directions for each of turbulent components in 3-dimension space. Limited by the monitoring conditions, only two integral scales of turbulence are calculated in this paper, the longitudinal can be calculated as

$$L_u^x = \frac{1}{\sigma_u^2} \int_0^\infty R_{12}(x) dx \tag{16}$$

where $R_{12}(x)$ = the cross-correlation function of turbulent wind speeds at two different locations $u(x_1, y_1, z_1, t)$ and $u(x_1+x, y_1, z_1, t)$, t = time, and σ_u^2 = variance of turbulent wind speeds. The definition of lateral integral scale of turbulence is similar.

The estimate of turbulence scales depends significantly upon the length and the stationarity of the record being analyzed and usually varies widely from experiment to experiment [33]. However, it is

difficult to use equation (16) in practice because wind speeds must be measured at multiple locations simultaneously. In order the solve the problem, Taylor's hypothesis is applied and equation (16) can be rewritten as

$$L_u^x = \frac{U}{\sigma_u^2}\int_0^{\infty} R_u(\tau)dx \tag{17}$$

where $R_u(\tau)$ = autocorrelation function of turbulent velocity, thus only one measuring location need be implemented.

However, the error caused by Taylor's hypothesis will increase for equation (17), when the value of autocorrelation function becomes very small. Flay and Stevenson [34] suggested that the integral upper limit of equation (17) should be taken as $\tau_{0.05}$, that represents the shift time when $R_u(\tau)$ reduces to $0.05\sigma^2$, then equation (17) is revised as

$$L_u^x = \frac{U}{\sigma_u^2}\int_0^{\tau_{0.05}} R_u(\tau)dx \tag{18}$$

The time history of integral scale of turbulence is shown in Fig. 17, where each value is calculated using 10 min data. In eye region, the lateral integral scales of turbulence reduced obviously, but they increased significantly with a maximum value of 1059.7 m in the eyewall region. From 9:45 to 11:00, the lateral integral scales of turbulence became greater than the longitudinal one, indicating larger scales of lateral vortexes. In outskirt region II, both longitudinal and lateral integral scales of turbulence were small due to the weakness of wind intensities, but except for the peak value at about 12:20, which may be influenced by surrounding buildings. Xiao et al. [35] investigated the integral scales of turbulence based on four measured datasets of three typhoons, which are compared with those of typhoon Jongdari, as shown in Table 4. The integral scales of turbulence of this paper are close to those of typhoons Ryan and Sibyl.

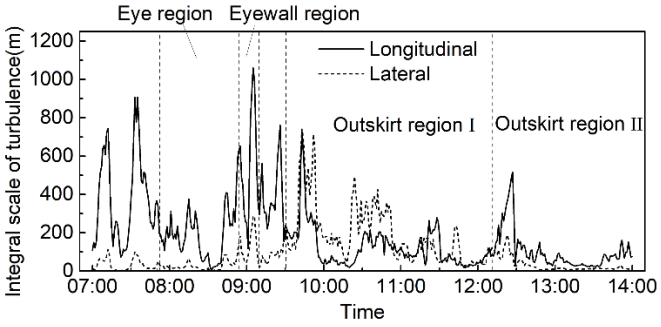

Fig. 17. Time history of turbulent integral scale

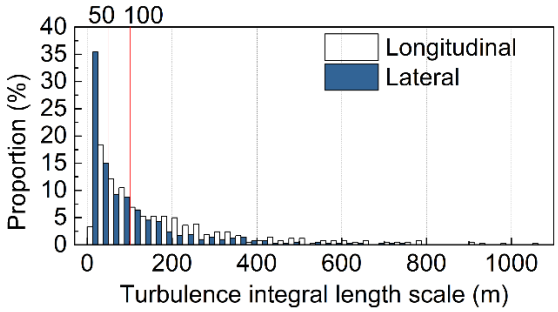

Fig. 18. Statistics of turbulent integral scale

Table 4. Integral scale of turbulence

Measured data	Measured height (m)	Mean L_u (m)	Range of L_u (m)	Mean L_v (m)	Range of L_v (m)	Maximum of 10-min mean wind speeds (m/s)
Outskirt region I	632	145.2	19.6~726.2	251.1	42.7~740.6	17.58
Outskirt region II	632	96.5	17.8~515.3	51.4	6.39~235.0	15.55
Eyewall region	632	573.2	116.2~1059.7	143.8	42.9~289.1	17.87
Eye region	632	155.8	8.4~374.5	24.1	1.1~86.8	6.1
Typhoon Ryan [35]	332	152	About 70~400	105	About 40~290	9.6
Typhoon Sibyl [35]	332	193	About 60~650	89	About 40~238	11.8
Typhoon Sally in Hong Kong [35]	332	279	About 90~780	179	About 55~395	14.6
Typhoon Sally in Shenzhen [35]	345	379	About 115~910	98	About 30~320	12.5

Fig. 18 shows the statistical distribution of integral scales of turbulence, the longitudinal one was mainly between 25 m and 225 m, and the lateral one distributed mostly between 25 m and 175 m. The horizontal size of the Shanghai Tower at the measured height is about 55 m, which is within the range of turbulent vortex scales, indicating that the turbulent wind of the typhoon may excite the structure relative violently.

4.2.4 The spectra of turbulent velocity

The recording time of the spectra of turbulent velocity should be equal to the duration of the strong winds in a typical storm, which is usually assumed to be 1 hour [33]. In order to analyze the evolution characteristics of the spectra of turbulent velocity, a moving time window with a width of 1 h was applied to the data to calculate the spectra in each time window and each moving step was 1 min. The results are indicated in Fig. 19. The change of turbulent energy can be illustrated from the variation of the spectra. As shown in Fig. 19, between 7:00 and 9:45, the energy of the longitudinal turbulent wind was mainly concentrated at 0.02 Hz, whereas that of the lateral one was concentrated at 1.0 Hz. From 9:45 to 12:10, the energy of longitudinal one was mostly concentrated near 0.5 Hz, but that of the lateral one was near 0.5 Hz or 0.03 Hz. From 12:10 to 14:00, the energy distribution of longitudinal turbulent wind did not change basically except for the sudden change at about 12:25 with the energy transferring to low frequency, which may be due to the decrease of wind speeds.

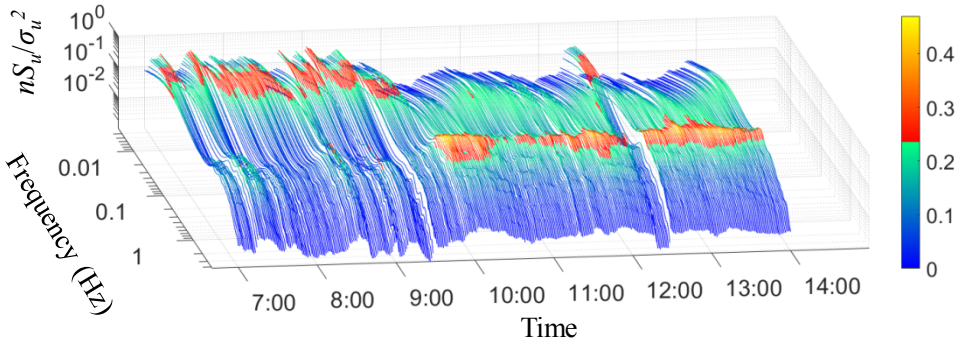

(a)

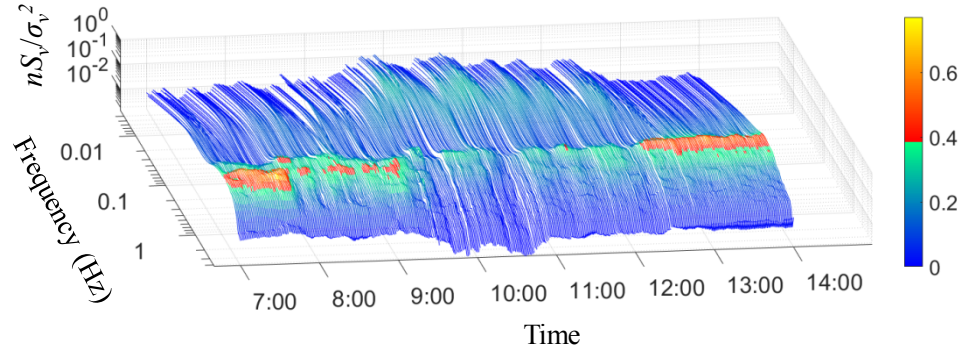

(b)

Fig. 19. Time histories of fluctuation wind power spectrum: (a) longitudinal direction; and (b) lateral direction

According to the assumption of isotropy of turbulent wind, a generalized power spectral density (PSD) was derived in Ref. [21], which is defined as follows.

Longitudinal direction:

$$\frac{nS_u(n)}{\sigma_u^2} = \frac{4f_u}{(1+\mathrm{A}f_u^{\,b})^c} \tag{19}$$

Lateral direction:

$$\frac{nS_v(n)}{\sigma_v^2} = \frac{4f_v(1+B(1+de)f_v^e)}{(1+Bf_v^e)^{d+1}} \tag{20}$$

where A, b, c, B, d, and e = the parameters to be fitted; n = frequency; $f_u = \frac{nL_u^x}{U}$; $f_v = \frac{nL_v^x}{U}$; S_u and S_v = PSDs of the turbulent wind in the longitudinal and lateral directions, respectively; and σ_u and σ_v = the RMSs of the fluctuating component in longitudinal and lateral directions, respectively. According to Kolmogrove's hypothesis [36], $S_u(n) \propto f^{-5/3}$ if $n \to \infty$, thus equation (19) can be modified as:

$$\frac{nS_u(n)}{\sigma_u^2} = \frac{4f_u}{(1+Af_u^b)^{\frac{5}{3b}}} \tag{21}$$

Given A = 70.8, b = 2, B = 283, d = 5/6, and e = 2, equations (24) and (22) become Von Karman spectrum. Data with relatively stable wind characteristics from 10:00 to 13:50 are selected to calculate the spectra and fitted using equations (20) and (21), with the results that A = 5.401, b = 0.982, B = 226.596, d = 0.880, and e =1.761.

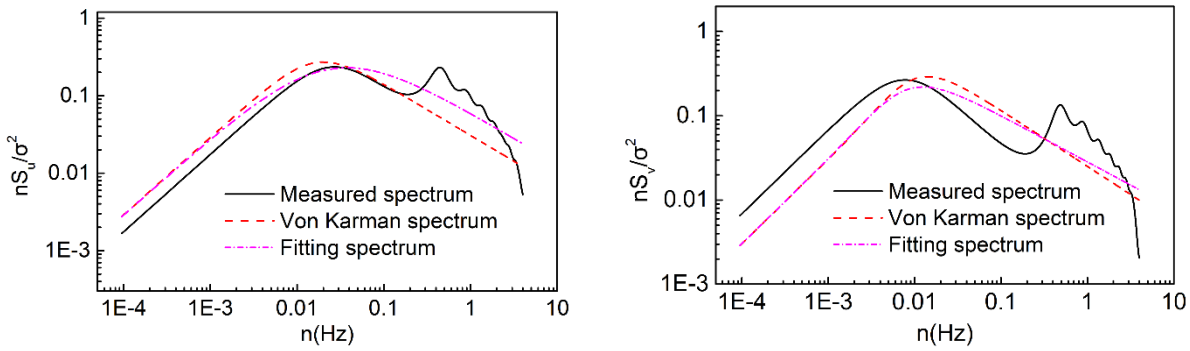

(a) (b)

Fig. 20. Fluctuation wind power spectrum of (a) longitudinal direction; and (b) lateral direction

Fig. 20 shows the comparison between measured, fitting, and Von Karman spectra. The longitudinal Von Karman spectrum is similar to the measured spectrum, and its value is slightly higher than the measured spectrum in the low frequency part. However, there are large differences in the lateral direction spectra, and the Von Karman spectrum is higher than the measured one. Based on the measured spectra, both the two direction spectra have one more peak in high frequency part and the lateral one is more prominent, as indicated in Fig. 20(b). Tamura [36] also found the two peaks phenomenon according to a measured wind speed before and after a typhoon center passed a certain place. It means that the spectrum characteristics of typhoon are different from those of normal wind. Unlike the streamlined bodies, the tall buildings are bluff against the flow, which could cause the flow to separate, rather than to follow body contours [37]. In addition, the disturbance of the wind field caused by the vortex shedding from the building itself may also cause two peaks in spectrum.

5. Conclusions

Based on the measured wind speed and direction atop the Shanghai Tower, the correlations of the mean wind speeds in different averaging times were analyzed using a non-stationary wind velocity model. The fluctuation wind characteristics at evolutional stages of the typhoon including turbulence intensity, gust factor, integral scale of turbulence and power spectrum were discussed and compared with several typhoons measured atop the other super-tall buildings. The relevant conclusions could provide useful information for the high altitude wind features in dense building landform and aid the wind-resistant

design of 600 m+ super-tall buildings. Some conclusions are drawn as follows:

(1) The method of the wavelet hard-threshold denoising, combined with moving window technology, can remove the abnormal value of data effectively, without altering the signal characteristics. However, it should be noted that the data of wind direction need to be "continuously transformed" before applying these preprocessing.

(2) There is a relatively stable ratio between the average wind speeds in 10 min and 1 hour duration time, e.g., $\overline{v}_{1h}$:$\overline{v}_{10min}$ = 0.962 : 1, and both of them can reflect the main change of wind velocity. Since 3 s mean wind speed is sensitive to samples, it is not suitable as duration time.

(3) During the period when the typhoon is stable, the longitudinal and lateral turbulence intensities decrease with the increase of the mean wind speeds, with the linear relationships of I_u = -0.879U + 0.771 and I_v = -0.044U + 0.761. The ratio of longitudinal turbulence intensity to the lateral one is 1:0.835 for most of the time. The turbulence intensities calculated by different measured samples are quite different, so the samples should be selected from the period with stable wind characteristics.

(4) Gust factors decrease with the mean wind speeds, and there exists linear relationships: Gu = -0.982U + 2.752 and Gv = -0.0833U + 1.178. There is a slight difference between the linear and nonlinear fitting of three longitudinal parameters, i.e. the gust factor, turbulence intensity and gust duration time, but obvious error exists as to the linear fitting of the lateral parameters. The nonlinear fitting results are safer for the bearing capacity design of the curtain structures.

(5) The integral scales of turbulence are larger than the horizontal size of the Shanghai Tower during most of the time of the typhoon, indicating that the wind may excite the structure relative violently. In addition, the spectra of turbulent velocity show various characteristics in different stages. Thus, it is necessary to pay attention to the evolution of wind field characteristics when analyzing the measured data of typhoon.

Acknowledgments

The research described in this paper was financially supported by National Natural Science Foundation of China (NSFC) (grant No. 51878475). The financial support is gratefully acknowledged.

References

[1] F.Q. Meng, B.J. He, J. Zhu, D.X. Zhao A. Darko, Z.Q. Zhao, Sensitivity analysis of wind pressure coefficients on CAARC standard tall buildings in CFD simulations, *Journal of Building Engineering*. 16 (2018) 146-158. https://doi.org/10.1016/j.jobe.2018.01.004.

[2] O.J. Andersen, J. Lovseth, Gale force maritime wind. The Frøya data base. Part I: Sites and instrumentation. Review of the data base, *Journal of Wind Engineering and Industrial Aerodynamics*. 57 (1) (1995) 97-109. https://doi.org/10.1016/0167-6105(94)00101-I.

[3] J.A. Wills, A. Grant, C.F. Boyack, Offshore mean wind profile, *Department of Energy, London, Offshore Technology Report*. OTH86-226, 1986. http://hdl.handle.net/10068/619666.

[4] X. Wang, P. Huang, X.F. Yu, X.R. Wang, H.M. Liu, Wind characteristics near the ground during typhoon Meari, *Journal of Zhejiang University-Science A*. 18 (1) (2017) 33-48. https://doi.org/10.1631/jzus.A1500310.

[5] X. Wang, C. Huang, P. Huang, X. Yu, Study on wind characteristics of a strong typhoon in near-ground boundary layer, *Structural Design of Tall and Special Buildings*. 26 (5) (2017). https://doi.org/10.1002/tal.1338.

[6] L. Li, Y. Xiao, H. Zhou, F. Xing, L. Song, Turbulent wind characteristics in typhoon Hagupit based on field measurements, *International Journal of Distributed Sensor Networks*. 14 (10) (2018). https://doi.org/10.1177/1550147718805934.

[7] L.L. Song, Q.S. Li, W.C. Chen, P. Qin, H.H. Huang, Y.C. He, Wind characteristics of a strong typhoon in marine surface boundary layer, *Wind and Structures*. 15 (1) (2012) 1-15.

https://doi.org/10.12989/was.2012.15.1.001.
[8] J.M.W Brownjohn, T.C. Pan, H.K. Cheong, Dynamic response of Republic Plaza, Singapore, *Structural Engineer London*. 76 (11) (1998) 221-226.
[9] Q.S. Li, L.H. Zhi, A.Y. Tuan, C.S. Kao, S.C. Su, C.F. Wu, Dynamic behavior of Taipei 101 Tower: Field measurement and numerical analysis, *Journal of Structural Engineering*. 137 (1) (2011) 143-155. https://doi.org/10.1061/(asce)st.1943-541x.0000264.
[10] T. Kijewski-Correa, D.K. Kwon, A. Kareem, A. Bentz, Y. Guo, S. Bobby, A. Abdelrazaq, SmartSync: An integrated real-time structural health monitoring and structural identification system for tall buildings, *Journal of Structural Engineering*. 139 (10) (2013) 1675-1687. https://doi.org/10.1061/(ASCE)ST.1943-541X.0000560.
[11] J.P. Amezquita-Sanchez, H. Adeli, Signal processing techniques for vibration-based health monitoring of smart structures, *Archives of Computational Methods in Engineering*. 23 (1) (2016) 1-15. https://doi.org/10.1007/s11831-014-9135-7.
[12] T. Liu, B. Yang, Q.L. Zhang, Health monitoring system developed for Tianjin 117 high-rise building, *Journal of Aerospace Engineering*. 30 (2) (2017). https://doi.org/10.1061/(ASCE)AS.1943-5525.0000602.
[13] Q.S. Li, Y.Q. Xiao, J.R. Wu, J.Y. Fu, Z.N. Li, Typhoon effects on super-tall buildings, *Journal of Sound and Vibration*. 313 (3-5) (2008) 581-602. https://doi.org/10.1016/j.jsv.2007.11.059.
[14] Q.S. Li, X. Li, Y. He, J. Yi, Observation of wind fields over different terrains and wind effects on a super-tall building during a severe typhoon and verification of wind tunnel predictions, *Journal of Wind Engineering and Industrial Aerodynamics*. 162 (2017) 73-84. https://doi.org/10.1016/j.jweia.2017.01.008.
[15] X. Li, Q.S. Li. Monitoring structural performance of a supertall building during 14 tropical cyclones, *Journal of Structural Engineering*. 144 (10) (2018) 04018176. https://doi.org/10.1061/(ASCE)ST.1943-541X.0002145.
[16] Q.S. Li, Y.C. He, Y.H. He, K. Zhou, X.L. Han, Monitoring wind effects of a landfall typhoon on a 600 m high skyscraper, *Structure and Infrastructure Engineering*. 15 (1) (2019) 54-71. https://doi.org/10.1080/15732479.2018.1505923.
[17] C.Q. Wang, Z.N. Li, Q.Z. Luo, L. Hu, Z.F. Zhao, J.X. Hu, X.W. Zhang, Wind characteristics investigation on the roofs of three adjacent high-rise buildings in a coastal area during typhoon Meranti, *Applied Sciences-Basel*. 9 (3) (2019). https://doi.org/10.3390/app9030367.
[18] M.D. Powell, S.H. Houston, T.A. Reinhold, Hurricane Andrew's landfall in south Florida. Part I: Standardizing measurements for documentation of surface wind fields, *Weather and Forecasting*. 11 (3) (1996) 304-328. https://doi.org/10.1175/1520-0434(1996)011<0304:HALISF>2.0.CO;2.
[19] Y. An, Y. Quan, M. Gu. Field measurement of wind characteristics of typhoon Muifa on the Shanghai World Financial Center, *International Journal of Distributed Sensor Networks*. (2012). https://doi.org/10.1155/2012/893739.
[20] Y. Quan, S. Wang, M. Gu, J. Kuang, Field measurement of wind speeds and wind-induced responses atop the Shanghai World Financial Center under normal climate conditions, *Mathematical Problems in Engineering*. (2013). http://doi.org/10.1155/2013/902643.
[21] Z.F. Huang. M. Gu, Field measurement of wind characteristics of typhoon Chan-hom on Shanghai World Financial Center, *Journal of Tongji University (Natural Science)*. 44 (8) (2016) 1205-1211. https://doi.org/10.11908/j.issn.0253-374x.2016.08.010.
[22] J. Wu, H.J. Xu, Q.L. Zhang, Dynamic performance evaluation of Shanghai Tower under winds based on full-scale data, *Structural Design of Tall and Special Buildings*. 28 (9) (2019). http://doi.org/10.1002/tal.1611.
[23] Q.S. Li, X. Li, Y.C. He, Monitoring wind characteristics and structural performance of a supertall building during a landfall typhoon, *Journal of Structural Engineering*. 142(11) (2016) 04016097. https://10.1061/(ASCE)ST.1943-541X.0001564.
[24] Q. Zhang, X. Tang, J. Wu, B. Yang, Online automatic structural health assessment of the Shanghai Tower, *Smart Structures and Systems*. 24 (3) (2019) 319-332. https://doi.org/10.12989/sss.2019.24.3.319.
[25] F. Rizzo, F. Ricciardelli, G. Maddaloni, A. Bonati, A. Occhiuzzi. Experimental error analysis of dynamic properties for a reduced-scale high-rise building model and implications on full-scale behavior, *Journal of*

Building Engineering. 28 (2020) 101067. https://doi.org/10.1016/j.jobe.2019.101067.
[26] S.K. Au, F.L. Zhang, P. To, Field observations on modal properties of two tall buildings under strong wind, *Journal of Wind Engineering and Industrial Aerodynamics*, 101 (2012) 12-23. https://doi.org/10.1016/j.jweia.2011.12.002.
[27] F.L. Zhang, H.B. Xiong, W.X. Shi, X. Ou, Structural health monitoring of Shanghai Tower during different stages using a Bayesian approach, *Structural Control and Health Monitoring*. 23 (2016) 1366-1384. https://doi.org/10.1002/stc.1840.
[28] J.Y. Fu, J.R. Wu, A. Xu, Q.S. Li, Y.Q. Xiao, Full-scale measurements of wind effects on Guangzhou West Tower, *Engineering Structures*. 35 (2012) 120-139. https://doi.org/10.1016/j.engstruct.2011.10.022.
[29] K. Wijesooriya, D. Mohotti, K. Chauhan, D. Dias-da-Costa. Numerical investigation of scale resolved turbulence models (LES, ELES and DDES) in the assessment of wind effects on supertall structures, *Journal of Building Engineering*. 25 (2019). https://doi.org/10.1016/j.jobe.2019.100842.
[30] Z.K. Wu, L. Zhao, L.D. Zhu, Y.J. Ge. Hight-altitude observation about turbulence characteristics for "Krose" (0716) strong typhoon, *Acta Aerodynamica Sinica*, 28 (3) (2010) 291-296. https://doi.org/10.3969/j.issn.0258-1825.2010.03.009.
[31] H. Ishizaki, Wind profiles, turbulence intensities and gust factors for design in typhoon-prone regions, *Journal of Wind Engineering & Industrial Aerodynamics*. 13 (1) (1983) 55-66. https://doi.org/10.1016/0167-6105(83)90128-9.
[32] E.C.C. Choi, Gradient height and velocity profile during typhoons, *Journal of Wind Engineering and Industrial Aerodynamics*. 13 (1) (1983) 31-41. https://doi.org/10.1016/0167-6105(83)90126-5.
[33] E. Simiu, R.H. Scanlan. Wind effects on structures. New York: Wiley, 1996.
[34] R.G. Flay, D.C. Stevenson. Integral length scales in strong winds below 20 m, *Journal of Wind Engineering and Industrial Aerodynamics*. 28 (1-3) (1988) 21-30. https://doi.org/10.1016/0167-6105(88)90098-0.
[35] Y.Q. Xiao, J. C. Sun, Q.S. Li, Turbulent integral scale and fluctuation wind speed spectrum of typhoon: an analysis based on field measurements, *Journal of Natural Disasters*. 15 (5) (2006) 45-53. https://doi.org/10.3969/j.issn.1004-4574.2006.05.008.
[36] Y. Tamura, A. Kareem. Advanced structural wind engineering, *Springer*, Japan, 2013. https://doi.org/10.1007/978-4-431-54337-4.
[37] A. Sharma, H. Mittal, A. Gairola, Mitigation of wind load on tall buildings through aerodynamic modifications: Review, *Journal of Building Engineering*. 18 (2018) 180-194. https://doi.org/10.1016/j.jobe.2018.03.005.

Highlights

- Wind characteristics of 600 m+ super-tall building during a typhoon are obtained
- Information for wind-resistant design of 600 m+ super-tall buildings is provided
- Fluctuation wind characteristics are discussed and compared with other typhoons
- Turbulence intensities calculated by different measured samples are quite diverse
- Spectra of turbulent velocity show various characteristics in different stages

Wind characteristics atop Shanghai Tower during typhoon Jongdari using field monitoring data

Jie Wu[a], Ningtao Hu[a], You Dong[b], Qilin Zhang[a], Bin Yang[a]

[a] *College of Civil Engineering, Tongji University, 1239 Siping Road, Shanghai 200092, PR China*

[b] *Department of Civil and Environmental Engineering, The Hong Kong Polytechnic University, Hong Kong, PR China*

Abstract: In this paper, detailed analysis of the field wind data atop the Shanghai Tower is conducted to investigate the wind characteristics evolution generated by typhoon Jongdari, which could provide useful information for the high altitude wind features in dense building landform and aid the wind-resistant design of 600 m+ super-tall buildings. The necessity of data preprocessing is discussed and some precautions for processing the wind directions are pointed out. The correlations of the mean wind speeds in different averaging times are analyzed using a non-stationary wind velocity model. The fluctuation wind characteristics at evolutional stages of the typhoon including turbulence intensity, gust factor, integral scale of turbulence and power spectrum are discussed and compared with several typhoons measured atop the other super-tall buildings. Based on the analysis, the ratio of the mean wind speeds between 10 min and 1 h averaging times remains stable. It is found that there is a slight difference between the linear and nonlinear fitting of three longitudinal parameters, i.e. the gust factor, turbulence intensity and gust duration time, but obvious error exists as to the linear fitting of the lateral parameters. The statistical results of the turbulent integral scale reflect relatively violent excitation of the turbulent wind to the structure and the spectra of turbulent velocity are associated with various characteristics in different stages of the typhoon.

Key words: wind characteristics; field monitoring; typhoon; super-tall building; Shanghai Tower

1. Introduction

In recent years, increasing demands for residential space have led to a large number of high-rise buildings especially in some coastal areas, where are often vulnerable to strong winds. Therefore, wind characteristics and typhoon evolution are of great significance for wind-resistance design and disaster prevention of these high-rise buildings. Due to the particularity of structure and mechanism of typhoons and the influence of bluff body flow around high-density buildings, it is difficult for wind tunnel to simulate complex wind characteristics in high-rise building groups. Therefore, field monitoring becomes the most direct and reliable means to investigate the characteristics. These measurements have supplied people with real wind loads which have inherently included full complexity [1]. In the past few decades, researches in different countries have established the relevant wind databases by measurements, such as Norway's Froya database [2], Canada's and Britain's near sea wind observation database [3], etc.

Wind data are often monitored from wind observation towers in the field of meteorology. By monitoring at four heights of a 40-m tower, Wang et al. [4,5] investigated turbulence characteristics including wind-speed profiles, turbulence integral scales, power spectra, correlations, and coherences during typhoon Meari and Muifa (2011). Based on the field monitoring on a 100-m high tower, Li et al. [6] investigated wind characteristics of typhoon Hagupit (2008), and the relevant results were compared with that of typhoon Maemi (2003) and other three hurricanes. Song et al. [7] investigated Typhoon Hagupit (2008) in the marine surface boundary layer by observing from a 100-m high offshore meteorological tower. However, the wind towers are usually built on flat and wide terrain, that is different from urban complex one, the relevant measurements of wind characteristics associated with typhoons for super-tall buildings are relatively scarce, especially in dense building landform.

In the past decades, with the development of information technology and sensors, many super-tall buildings have been equipped with structural health monitoring (SHM) systems [8-12], which enabled people to monitor the environmental wind continuously atop building for a long time, obtaining the

valuable first-hand data. Guangdong-Hong Kong-Macao Greater Bay Area (BGA) always suffers from several typhoons every year, and it provides excellent opportunities to study the characteristics of typhoons in urban. Li et al. [13-16] analyzed the measured wind data atop numbers of super-tall buildings in BGA, such as Ping An International Finance Centre (592.5 m) in Shenzhen, the International Finance Centre (420 m) in Hong Kong, and CITIC Plaza Tower (391 m) in Guangzhou, including the characteristics of high-altitude wind field, wind load distribution and wind-induced response of the structure. Wang et al. [17] investigated the pulsating characteristics of three adjacent high-rise buildings under typhoon Moranti (2016).

Previous studies (e.g. Li et al. [14], Powell et al. [18]) indicated that the surface winds of a landfall tropical cyclone (TC) may be significantly affected by local topography. Shanghai, where several super-tall and many tall buildings were built in the past three decades, experiences fewer typhoons than BGA and the corresponding researches on measured data become particularly valuable. Based on the measured wind data atop Shanghai World Financial Center (492 m), An et al. [19] investigated the characteristics of typhoon Muifa (2011), Quan et al. [20] investigated the normal wind characteristics, and Huang and Gu [21] studied wind characteristics for typhoon Chan-hom (2015). Wu et al. [22] analyzed normal wind characteristics from the measured data atop the Shanghai Tower. In addition, the wind induced vibration of super-tall buildings has been widely investigated by the full-scale measurements and wind tunnel tests [23-25]. Au et.al [26] presented observations on the identified modal properties of two tall buildings using ambient vibration data collected during strong wind events. Zhang et al. [27] utilized the fast Bayesian method to analyze the ambient vibration data of the Shanghai Tower at different construction stages and identified the dynamic parameters of the structure. Fu et al. [28] evaluated the dynamic characteristics and wind effects on the Guangzhou West Tower. Although many measurements and theoretical researches on the wind characteristics and wind induced vibration under typhoon have been conducted, the studies on the high-altitude of the 600 m+ super-tall building are still scarce.

In this paper, the wind speeds and directions atop the Shanghai Tower under the influence of typhoon Jongdari are monitored and recorded. These data are preprocessed firstly to reduce the influence of outlier data and noise. In particular, some precautions for processing the wind directions are pointed out and a solution is put forward. Based on a non-stationary calculation model, the differences of mean wind in various average time are analyzed. In order to investigate the wind characteristics evolution under the investigated typhoon, the fluctuation wind characteristics at different stages are presented and discussed, such as turbulence intensity, gust factor, integral scale of turbulence and power spectrum. These analysis results are also compared with several typhoons measured atop other super-tall buildings. The relevant conclusions could provide useful information for the high altitude wind features in dense building landform and wind-resistant design of 600 m+ super-tall buildings.

2. Typhoon Jongdari and field measurement profile

Jongdari developed as a tropical depression in the northeast of the Pacific Ocean on July 25, 2018, and made landfall over Jinshan coast, Shanghai, at about 10:30 on August 3 as a tropical storm with the maximum wind force of 9th grade (in Beaufort Scale, 23 m / s) near its center and the minimum central pressure of 985 hPa. Later, it continued to move along the northwest direction and weakened gradually into the tropical depression. At 23:00 the wind-rain intensity decreased and National Meteorological Center of CMA (China) stopped numbering it.

(a) (b)

Fig. 1. Path of typhoon Jongdari. (a) Typhoon center track; (b) Shanghai tower

The Shanghai Tower, located in Lujiazui, Shanghai, China, is the second tallest building in the world with a height of 632 m. It consists of a 121-story main building, a 5-story podium building, and a 5-story basement. As shown in Fig 1 (b), it is surrounded by several super-tall and many tall buildings, which belongs to a typical rough underlying surface of urban, making the wind field characteristics complex. As shown in Fig. 2, an ultrasonic anemometer with an acquisition sampling rate (ASR) of 100Hz is installed atop the building. The specific parameters of the anemometer are listed in Table 1.

Table 1. Specific parameters of ultrasonic anemometer

Wind speed parameter	Technical index	Wind direction parameter	Technical index
Range	0 ~ 40m	Range of wind direction	0.0 ~ 359.9º
Resolving power	0.1 m/s	Range of angle	± 60 º
Threshold	0.01 m/s	Resolving power	0.1 º
Precision	±1% rms ± 0.05 m/s	Precision	± 2 º(1 ~ 30 m/s)

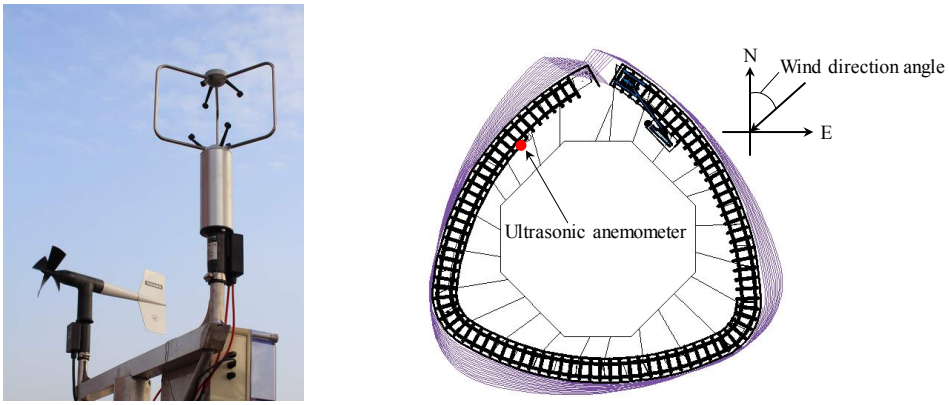

Fig. 2. Ultrasonic anemometer and its installation location

3. Data preprocessing

The data from 7:00 to 14:00 on August 3, 2018, were used to analyze the basic characteristics of the typhoon. Since the ultrasonic anemometer determines the airflow velocity by time difference along ultrasonic propagation path, any substances obstructing the path would reduce its accuracy, resulting in outlier data (or abnormal value). For the purpose of judging and eliminating these outliers, a method, which combined with a moving window and threshold of 3 times standard deviation, is used to preprocess the data. Meanwhile, the sensor is inevitably suffered from external interference during its work, hence it is necessary to denoise the signal (or data). In general, denoise methods include commonly filter technologies, Kalman filtering, empirical mode decomposition (EMD) and wavelet denoising. In this paper, a wavelet hard-threshold denoising method is utilized by adopting Sym4

wavelet. Sym4 wavelet is orthogonal and compactly supported, which can reduce a certain phase distortion of signal decomposition and reconstruction.

It should be paid special attention in dealing with the data of wind directions. When the two wind directions of adjacent time are in A and B respectively as shown in Fig.3, there are two possibilities for the change routes: ② and ①, which, obviously, is more likely. If the above-mentioned preprocessing is directly applied for the data of wind directions, it is very possible to change along route ②. Therefore, a "continuity conversion" is carried out before the preprocessing being applied. The wind direction at the time i is denoted by $\alpha(i)$, and the "continuity conversion" goes as follows:

(1) If $\alpha(i) \geqslant 360^{\circ} - \beta$ and $\alpha(i+1) \leqslant \beta$, then $\alpha(i+1) = \alpha(i+1) + 360^{\circ}$; and

(2) If $\alpha(i) \leqslant \beta$ and $\alpha(i+1) \geqslant 360^{\circ} - \beta$, then $\alpha(i+1) = \alpha(i+1) - 360^{\circ}$.

where β needs to be assigned and equals 90° herein. In this way, the range of the data changes to $[-\beta, 360^{\circ} + \beta]$. After the "continuity conversion" and the outlier data being removed as well as denoise, the converted data need to be restored to original range, i.e., $\alpha(i) = \alpha(i) - 360^{\circ}$ for $\alpha(i) > 360^{\circ}$, and $\alpha(i) = \alpha(i) + 360^{\circ}$ for $\alpha(i) < 0^{\circ}$.

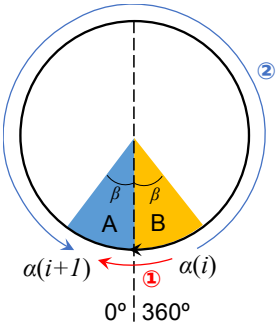

Fig. 3. Diagram for discontinuity of wind speeds

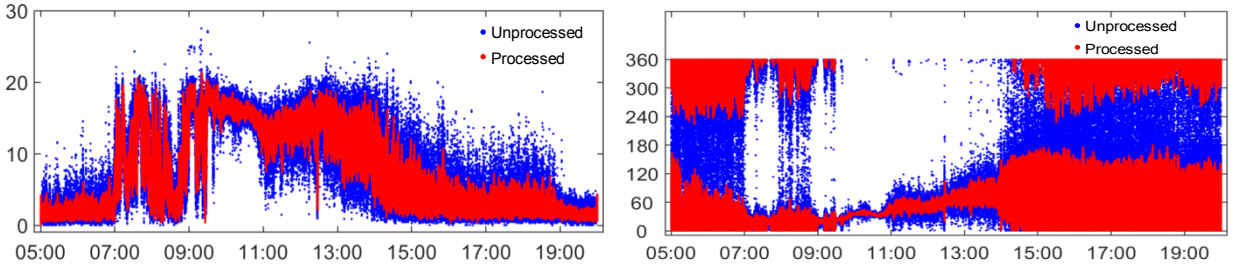

(a) (b)

Fig. 4. Unprocessed and processed (a) wind speeds; and (b) wind directions

Fig. 4 shows the comparison of wind data before and after preprocessing (including outlier data processing and wavelet hard-threshold denoising). It can be seen that the above processing methods can remove the abnormal value effectively without altering the signal features. As shown in Fig. 4 (a), the wind speeds were relatively high from 7:30 to 8:00 but became low with violent fluctuation of wind directions from 8:20 to 8:50, and then increased sharply until tended to be stable after 8:55. The measured instantaneous maximum wind speed occurred between 8:50 and 9:10, reaching at 25.8 m/s.

4. Analysis of wind characteristics

Structural wind engineering mainly focuses on the wind characteristics of the atmospheric boundary layer, consisting of the averaging and fluctuation components. In this paper, the characteristics of the typhoon Jongdari are analyzed based on a non-stationary wind velocity model, including mean wind speed and direction, turbulence intensity, gust factor, integral scale of turbulence, and the spectra of turbulent velocity.

4.1 Mean wind speed and direction

For traditional analysis method, wind velocity is regarded hypothetically as a stationary random process and can be divided into constant component and fluctuating one, which stands for a stationary wind velocity model. This is reasonable for normal wind on open terrain. However, the wind velocity of typhoon, as a strong cyclonic airflow, is a non-stationary process. Therefore, the mean wind speeds are calculated combined with a moving window in time to establish a non-stationary wind velocity model. This model can diminish the deviation of wind characteristics due to different ways of segmentation sections in the stationary one. Each moving time step is assigned by 1 min, so one point can be obtained per minute. The model is described as follows.

In three-dimensional airflow, the wind velocity vector in the horizontal direction can be decomposed into two perpendicular components of X and Y directions. Wind speed at the time i is denoted by $V(i)$ and the incoming wind direction angle is denoted by $\alpha(i)$. To obtain the mean wind speeds and directions, a Cartesian coordinate system is established firstly to decompose the wind velocity into X and Y components:

$$u_x(i) = V(i)\cos\alpha(i) \tag{1}$$

$$u_y(i) = V(i)\sin\alpha(i) \tag{2}$$

$$\overline{u}_x(k) = \frac{1}{N_s}\sum_{i=1}^{N}\Omega(i-k)u_x(i) \tag{3}$$

$$\overline{u}_y(k) = \frac{1}{N_s}\sum_{i=1}^{N}\Omega(i-k)u_y(i) \tag{4}$$

where $\overline{u}_x$ and $\overline{u}_y$ = mean wind speeds in X and Y directions at the time k, respectively, N = the number of data points, and $\Omega(\bullet)$ represents rectangular window function:

$$\Omega(i) = \begin{cases} 1, & i \in [-\frac{N_s}{2}, \frac{N_s}{2}] \\ 0, & \text{else} \end{cases} \tag{5}$$

where N_s = the width of rectangular window. The mean wind speed denoted by $U(k)$ and the mean wind direction angle denoted by $D(k)$ can be calculated as follows:

$$U(k) = \sqrt{\overline{u}_x^2(k) + \overline{u}_y^2(k)} \tag{6}$$

$$D(k) = \begin{cases} \arctan\left(\dfrac{\overline{u}_x(k)}{\overline{u}_y(k)}\right) + H(-\overline{u}_x(k))\times 180°, & \overline{u}_y(k) \neq 0 \\ 90° + H(-\overline{u}_x(k))\times 180°, & \overline{u}_y(k) = 0 \end{cases} \tag{7}$$

if D < 0, then D = D + 360^o , where $H(\bullet)$ is Heaviside step function:

$$H(i) = \begin{cases} 1, & i \geq 0 \\ 0, & \text{else} \end{cases} \tag{8}$$

The longitudinal fluctuating wind speed denoted $u(i)$ and the lateral one denoted $v(i)$ are respectively:

$$u(i) = u_x(i)\sin D(k) + u_y(i)\cos D(k) - U(k) \tag{9}$$

$$v(i) = -u_x(i)\cos D(k) + u_y(i)\sin D(k) \tag{10}$$

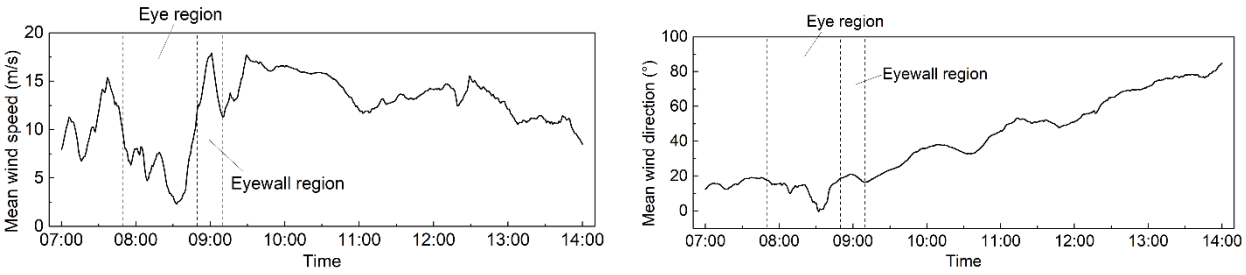

(a) (b)

Fig. 5. Time history of 10 min mean (a) wind speeds; and (b) wind directions

Fig.5 plots the time history of the 10 min mean wind speeds and directions. From 7:50 to 8:50 the mean wind speeds decreased obviously, which means that the typhoon eye was passing by. The maximum mean wind speed before the coming of typhoon eye reached 15.4 m/s, with the wind direction about 21°. After the eye, the mean wind directions changed from 20° to 80° gradually. From 8:55 to 9:08, the eyewall came when the mean wind speeds reached the maximum value of 17.9 m/s and the wind speeds became weakening slightly after 10:30.

The duration time of mean wind speed varies among different countries. For example, 3 s is adopted in Britain and Australia, 1 h in Canada, 10 min in China and Denmark, but the instantaneous maximum wind speed is used in Japan. Herein, for the investigated case, the mean wind speeds are volatile and high within 3 s average time (Fig. 6 (a)), but they are relatively stable and small within 10 min and 1 hour average time (Fig. 6 (b)).The detailed results are shown in Fig. 6.

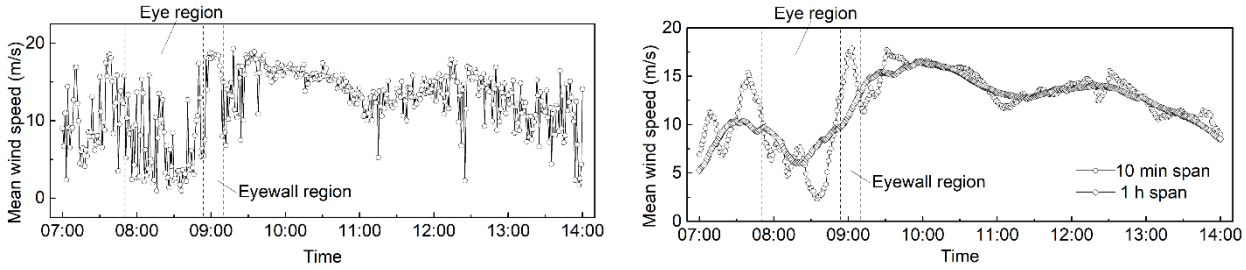

(a) (b)

Fig. 6. Mean wind speeds within time of (a) 3 s; and (b) 10 min and 1 h

To assess the correlation of the mean wind speeds within various averaging times, the linear fitting with zero intercept is carried out, and the results are indicated in Fig. 7. The Pearson coefficient of mean wind speeds between 1 hour and 10 min is 0.989, and that between 3 s and 10 min is 0.979, both of which indicate a linear correlation.

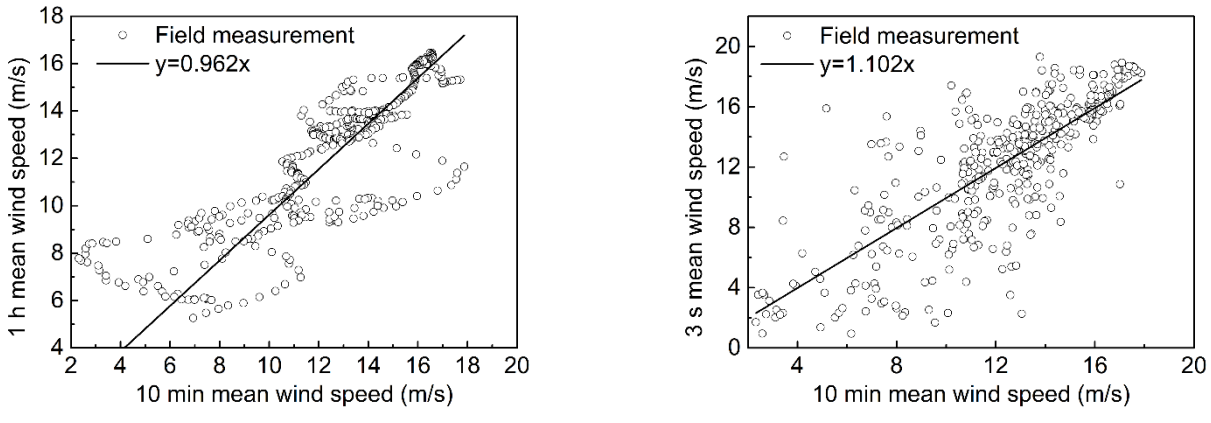

(a) (b)

Fig. 7. Correlation of the mean wind speeds within (a) 1 h and 10 min; and (b) 3 s and 10 min

The correlations of the mean wind speeds within various averaging times are compared with those of Ref. [21], as listed in Table 2. The correlation of 1 hour to 10 min in this paper is similar to that in Ref. [21], whereas that of 3 s to 10 min has a deviation of -8.6%. It indicates that 3 s is not a suitable averaging time due to its instability. However, the mean wind speeds within both 10 min and 1 hour reflect the main change of wind speeds well. Considering a larger amount of data required for 1 hour, 10 min could be selected for the computational process of wind speed.

Table 2. Correlations of average wind speeds within different duration time periods

Correlations	Ref. [21]	This paper	Deviation
$\overline{v}_{1h}$:$\overline{v}_{10min}$	0.953:1	0.962:1	0.94%
$\overline{v}_{3s}$:$\overline{v}_{10min}$	1.206:1	1.102:1	-8.6%

4.2 Characteristics of fluctuating wind

Fluctuating components of flow play an important role in the dynamics of the structure especially for tall buildings [29]. Flexible structures may exhibit resonant amplification effects and the aerodynamic behavior of structures may depend strongly upon the turbulence in the airflow. The features of the atmospheric turbulence include customarily turbulence intensity, gust factor, integral scale of turbulence, the spectra of turbulent velocity fluctuations, etc.

4.2.1 Turbulence intensity

Turbulence intensity describes the relative intensity of fluctuating wind and can be determined by the following equation:

$$I_i = \frac{\sigma_i}{U}, i = u, v \tag{11}$$

where σ_i = root mean square (RMS) of the fluctuating component in direction i, u denotes longitudinal direction, and v denotes lateral one.

The 10 min duration time is adopted to calculate the turbulence intensities herein, the time history of which is plotted in Fig. 8. It can be seen that the turbulence intensities perform obvious evolutions during different stages, including successively eye region, eyewall region, and outskirt regions. For the convenience of description, the period of 9:30-12:10 is denoted by outskirt region I and that of 12:10-14:00 is denoted by outskirt region II. Turbulence intensity of each stage of typhoon Jongdari is compared with that of typhoon Muifa [19], Chan-hom [21] in Shanghai, Imbudo [13] in Shenzhen, and the normal wind [30] measured atop the Shanghai World Financial Center, as listed in Table 3.

As shown in Fig. 8 and Table 3, the longitudinal turbulence intensities are greater than the lateral ones. In outskirt region I, the turbulence intensities are relatively stable but leap at about 11:00, which may be attributed to the change of wind directions (see Fig. 5 (a)) and be influenced by the obstructing of surrounding buildings. In this region, both longitudinal and lateral turbulence intensities are small, close to that of typhoon Chan-hom [21]. In outskirt region II, both longitudinal and lateral turbulence intensities increase. Longitudinal turbulence intensities are close to those of eyewall region, but the lateral ones are significantly different. In eye region, turbulence intensities increase due to low wind speeds. In eyewall region, the turbulence intensities reduce to a minimum of 0.0865, which is close to the normal wind [30].

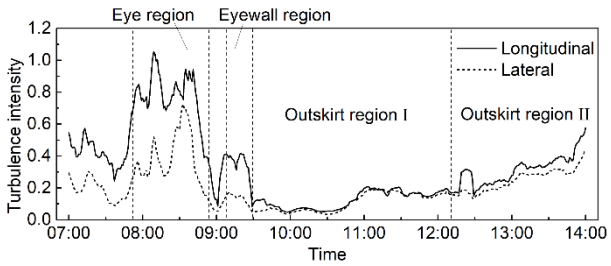

Fig. 8. Time history of turbulence intensity

Table 3. Comparison of turbulence intensities

Measured data	Measured height (m)	Mean of I_u	Range of I_u	Mean of I_v	Range of I_v	I_u:I_v
Outskirt region I	632	0.0968	0.0485~0.209	0.0774	0.0335~0.192	1:0.800
Outskirt region II	632	0.263	0.145~0.577	0.219	0.132~0.436	1:0.833
Eyewall region	632	0.26	0.0865~0.413	0.0896	0.0523~0.153	1:0.345
Eye region	632	0.815	0.596~1.054	0.421	0.212~0.725	1:0.517
Typhoons Muifa [19]	494	0.14	0.05~0.29	0.13	0.04~0.26	1:0.929
Typhoon Chan-hom [21]	494	0.107	0.061~0.155	0.066	0.040~0.158	1:0.617
Typhoon Imbudo [13]	345	0.196	-	0.112	-	1:0.571
Normal wind [30]	436	0.201	-	0.066	-	1:0.328

Figs. 9 (a) and 9 (b) show the variation of turbulence intensities with mean wind speeds. The Pearson coefficient between longitudinal turbulence intensities and average wind speeds is - 0.879 and that of lateral one is - 0.929, both of which are close to -1, indicating negative linear correlation: I_u = - 0.879 U + 0.771, I_v = -0.044 U + 0.761. Fig.9 (c) shows the correlation between longitudinal and lateral turbulence intensities from 10:00 to 13:50, while wind speed is relatively stable. Their Pearson coefficient is 0.993. According to linear fitting without intercept, there is a ratio of I_u : I_v = 1 : 0.835, which is close to that for both in outskirt regions I and II. Meanwhile, it is closest to that of typhoon Muifa [19] shown in Table 3, but quite different from that of typhoon Chan-hom [21] and Imbudo [13], which may due to the fact that these ratios were calculated by the measured data in the whole typhoon duration. In fact, it is unreasonable to use one value to represent the characteristics of turbulence intensities during the whole process of typhoon while the wind characteristics change greatly. Therefore, the data should be selected during the process when the wind characteristics are relatively stable. In this way, the computed turbulence intensities can describe the wind characteristics of the corresponding period accurately.

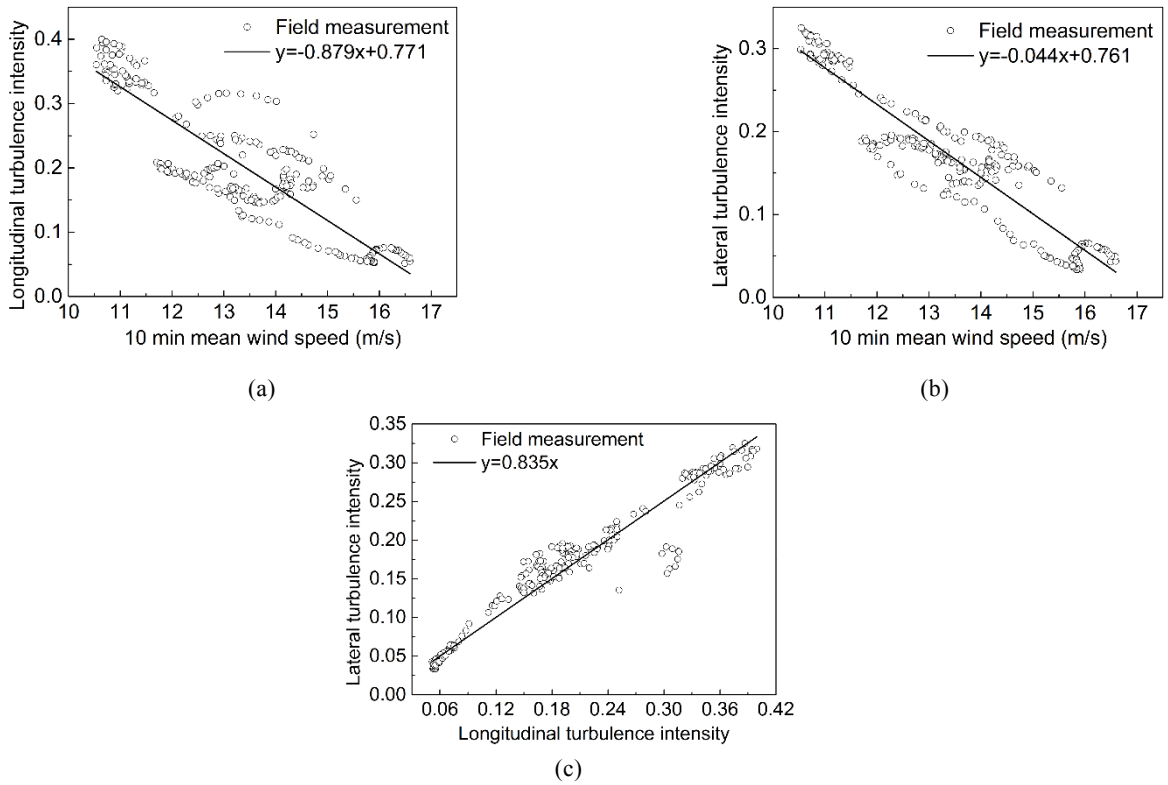

Fig. 9. Variations of (a) longitudinal turbulence intensities with mean wind speeds; (b) lateral turbulence intensities with mean wind speeds; and (c) lateral turbulence intensities with the longitudinal one

4.2.2 Gust factor

To consider the influence of gusting wind, the mean wind pressure or mean wind pressure coefficient is often used to predict the peak pressure on the surface of some cladding and enclosure structures, hence the gust factor should be calculated. Gust factor is defined as the ratio of the peak gust speed over a short duration t_g to the mean wind speed U in a relatively longer duration T.

Longitudinal gust factor:

$$G_u(t_g,T)=\frac{U(T)+u_g(t_g)}{U(T)}=1+\frac{u_g(t_g)}{U(T)} \tag{12}$$

Lateral gust factor:

$$G_v(t_g,T)=\frac{v_g(t_g)}{U(T)} \tag{13}$$

where u_g and v_g = the maxima of longitudinal and lateral mean wind speeds in duration t_g, respectively. In this paper, t_g = 3 s and T = 10 min.

As shown in Fig. 10, the gust factors reached at maximum when the typhoon eye passed through, decreased obviously in the eyewall region, and tended to be relatively stable in outskirt region.

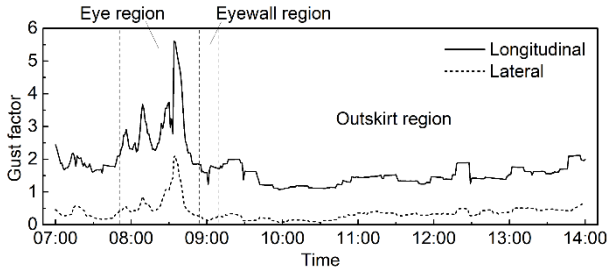

Fig. 10. Time history of gust factors

Herein, gust factors are obtained from the data between 10:00 and 13:50, while the wind characteristics were stable. Fig. 11 shows the linear correlation between the gust factors and the mean wind speeds: G_u = -0.982U + 2.752 with the Pearson coefficient of -0.763, and G_v = -0.0833U + 1.178 with the Pearson coefficient of -0.864.

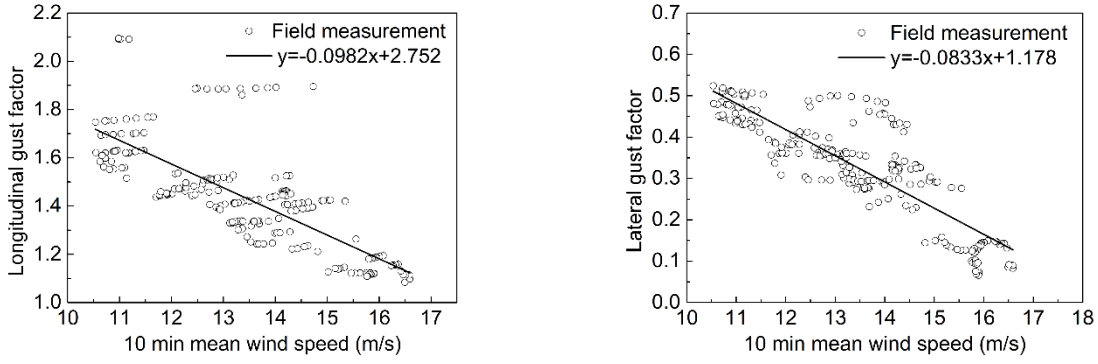

(a) (b)

Fig. 11. Variation of gust factors with mean wind speeds: (a) longitudinal direction; and (b) lateral direction

Ishizaki [31] suggested that the relationship between G_u, I_u, and t_g can be expressed by following equation:

$$G_u(t_g)=1+aI_u^b\ln(\frac{T}{t_g}) \tag{14}$$

where a and b = the parameters to be fitted, T = 10 min. Best fitting with this equation leads to

$G_u(t_g) = 1 + 0.339 I_u^{0.804} \ln(\frac{600}{t_g})$, as shown in Fig. 12.

Ishizaki [31] fitted the equation (14) with duration time of 10 min and 1 h, respectively, and suggested that a = 0.5 and b = 1.0, which means a linear relationship between G_u and I_u for each t_g. Choi [32] fitted the equation with duration time of 1 h and the results were a = 0.63 and b = 1.27, which indicates a nonlinear relationship. Fig. 13 shows the comparison between the results in this paper and those suggested by Ishizaki as well as Choi. The G_u of this paper is larger than that of Choi for I_u<0.278, but smaller than that for I_u > 0.278. However, the G_u of Ishizaki is just between those of this paper and Choi.

Fig. 14 (a) shows the linear and nonlinear fittings of G_u, I_u, and t_g, and Fig. 14 (b) illustrates the deviations between them which are less than 10% overall. Quan et al. [20] compared the linear and nonlinear fittings for T = 10 min, t_g = 3 s with the founding that they are almost similar, which is consistent with the results from this paper. As shown in Fig. 14 (b), when t_g < 2 s, I_u < 0.03 or I_u > 0.4, the gust factors of nonlinear fitting are 5% smaller than those of linear fitting. For t_g > 3 s or t_g = 3 s, which is commonly used, the gust factors of nonlinear fitting are greater than those of linear fitting, which means a safer condition to bearing capacity design of the enclosure structures.

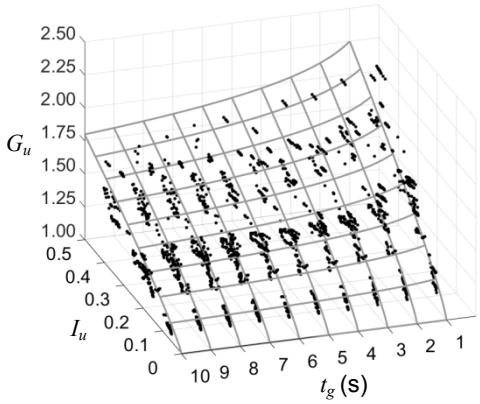

Fig. 12. Variation of longitudinal gust factors with turbulence intensities and gust duration time

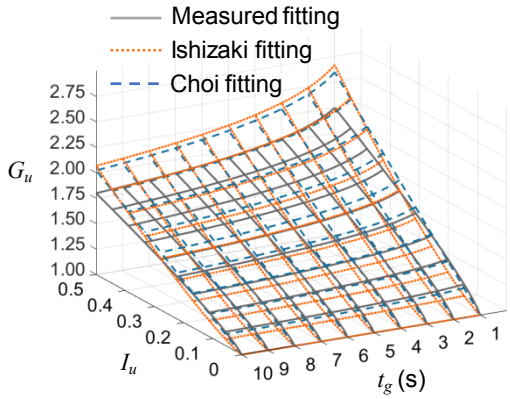

Fig. 13. Comparison of fitting results

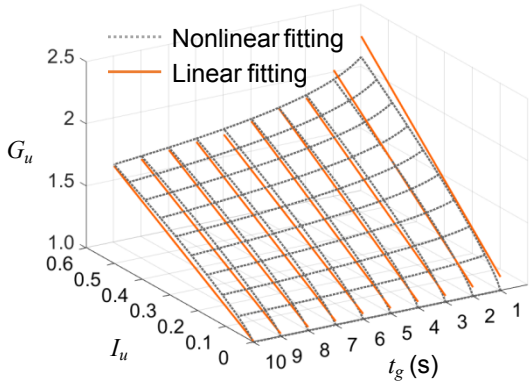

(a)

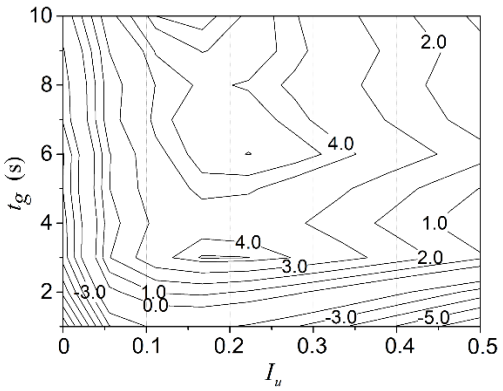

(b)

Fig. 14. Linear and nonlinear fitting of longitudinal gust factors with turbulence intensities and gust duration time: (a) comparison; and (b) deviation (%)

Similar with the definitions format of equation (14), relationship for G_v, I_v, and t_v can be defined as follows:

$$G_v(t_g) = cI_v^d \ln(\frac{600}{t_g}) \tag{15}$$

where c and d = parameters to be fitted. Fig. 15 shows the best fitting in this paper, with the result of

$$G_v(t_g) = 0.210 I_v^{0.656} \ln(\frac{600}{t_g}).$$

Both linear and nonlinear fittings are shown in Fig. 16 (a), and the deviations between them are illustrated in Fig. 16 (b). For $I_v > 0.25$, the gust factors of nonlinear fitting are much smaller than those of linear fitting. When $I_v < 0.25$ and $t_g \geq 3$ s, the gust factors of nonlinear fitting are larger than those of linear fitting with the maximum deviation of more than 80%. Therefore, the values of lateral gust factors may be smaller if they are converted from the turbulence intensities by linear fitting.

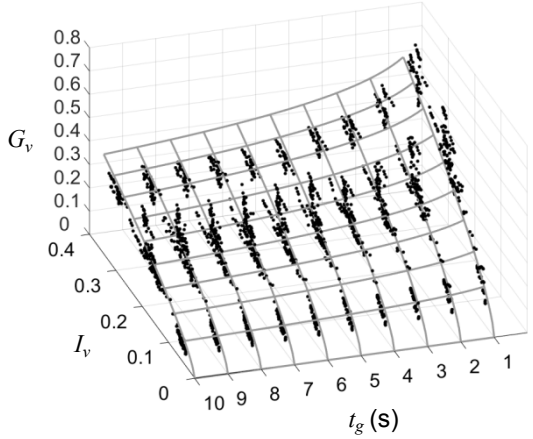

Fig. 15. Variation of lateral gust factors with turbulence intensities and gust duration time

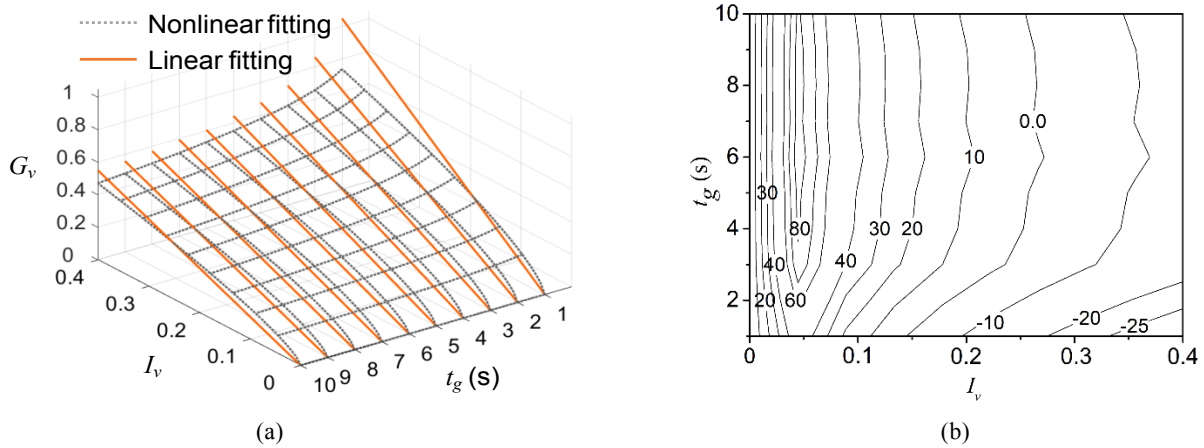

(a) (b)

Fig. 16. Linear and nonlinear fitting of lateral gust factors with turbulence intensities and gust duration time: (a) comparison; and (b) deviation (%)

4.2.3 Integral scale of turbulence

The velocity fluctuations of airflow passing a point would be caused by a superposition of eddies transported by the mean wind. Integral scale of turbulence can measure the average size of the turbulent eddies of the airflow. There are three vortex directions for each of turbulent components in 3-dimension space. Limited by the monitoring conditions, only two integral scales of turbulence are calculated in this paper, the longitudinal can be calculated as

$$L_u^x = \frac{1}{\sigma_u^2} \int_0^\infty R_{12}(x) dx \tag{16}$$

where $R_{12}(x)$ = the cross-correlation function of turbulent wind speeds at two different locations $u(x_1, y_1, z_1, t)$ and $u(x_1+x, y_1, z_1, t)$, t = time, and σ_u^2 = variance of turbulent wind speeds. The definition of lateral integral scale of turbulence is similar.

The estimate of turbulence scales depends significantly upon the length and the stationarity of the record being analyzed and usually varies widely from experiment to experiment [33]. However, it is

difficult to use equation (16) in practice because wind speeds must be measured at multiple locations simultaneously. In order the solve the problem, Taylor's hypothesis is applied and equation (16) can be rewritten as

$$L_u^x = \frac{U}{\sigma_u^2}\int_0^{\infty} R_u(\tau)dx \tag{17}$$

where $R_u(\tau)$ = autocorrelation function of turbulent velocity, thus only one measuring location need be implemented.

However, the error caused by Taylor's hypothesis will increase for equation (17), when the value of autocorrelation function becomes very small. Flay and Stevenson [34] suggested that the integral upper limit of equation (17) should be taken as $\tau_{0.05}$, that represents the shift time when $R_u(\tau)$ reduces to $0.05\sigma^2$, then equation (17) is revised as

$$L_u^x = \frac{U}{\sigma_u^2}\int_0^{\tau_{0.05}} R_u(\tau)dx \tag{18}$$

The time history of integral scale of turbulence is shown in Fig. 17, where each value is calculated using 10 min data. In eye region, the lateral integral scales of turbulence reduced obviously, but they increased significantly with a maximum value of 1059.7 m in the eyewall region. From 9:45 to 11:00, the lateral integral scales of turbulence became greater than the longitudinal one, indicating larger scales of lateral vortexes. In outskirt region II, both longitudinal and lateral integral scales of turbulence were small due to the weakness of wind intensities, but except for the peak value at about 12:20, which may be influenced by surrounding buildings. Xiao et al. [35] investigated the integral scales of turbulence based on four measured datasets of three typhoons, which are compared with those of typhoon Jongdari, as shown in Table 4. The integral scales of turbulence of this paper are close to those of typhoons Ryan and Sibyl.

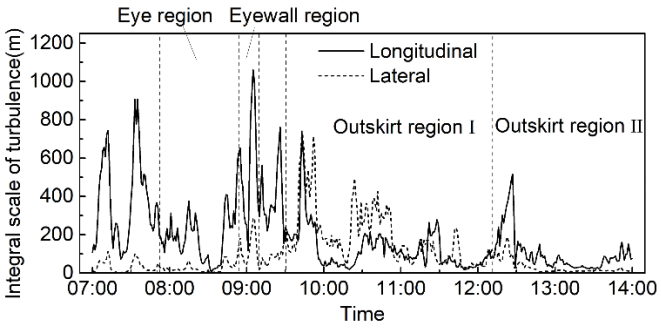

Fig. 17. Time history of turbulent integral scale

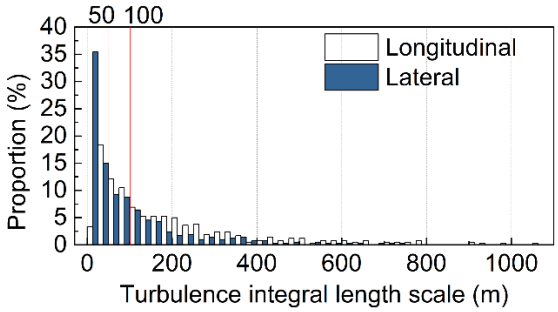

Fig. 18. Statistics of turbulent integral scale

Table 4. Integral scale of turbulence

Measured data	Measured height (m)	Mean L_u (m)	Range of L_u (m)	Mean L_v (m)	Range of L_v (m)	Maximum of 10-min mean wind speeds (m/s)
Outskirt region I	632	145.2	19.6~726.2	251.1	42.7~740.6	17.58
Outskirt region II	632	96.5	17.8~515.3	51.4	6.39~235.0	15.55
Eyewall region	632	573.2	116.2~1059.7	143.8	42.9~289.1	17.87
Eye region	632	155.8	8.4~374.5	24.1	1.1~86.8	6.1
Typhoon Ryan [35]	332	152	About 70~400	105	About 40~290	9.6
Typhoon Sibyl [35]	332	193	About 60~650	89	About 40~238	11.8
Typhoon Sally in Hong Kong [35]	332	279	About 90~780	179	About 55~395	14.6
Typhoon Sally in Shenzhen [35]	345	379	About 115~910	98	About 30~320	12.5

Fig. 18 shows the statistical distribution of integral scales of turbulence, the longitudinal one was mainly between 25 m and 225 m, and the lateral one distributed mostly between 25 m and 175 m. The horizontal size of the Shanghai Tower at the measured height is about 55 m, which is within the range of turbulent vortex scales, indicating that the turbulent wind of the typhoon may excite the structure relative violently.

4.2.4 The spectra of turbulent velocity

The recording time of the spectra of turbulent velocity should be equal to the duration of the strong winds in a typical storm, which is usually assumed to be 1 hour [33]. In order to analyze the evolution characteristics of the spectra of turbulent velocity, a moving time window with a width of 1 h was applied to the data to calculate the spectra in each time window and each moving step was 1 min. The results are indicated in Fig. 19. The change of turbulent energy can be illustrated from the variation of the spectra. As shown in Fig. 19, between 7:00 and 9:45, the energy of the longitudinal turbulent wind was mainly concentrated at 0.02 Hz, whereas that of the lateral one was concentrated at 1.0 Hz. From 9:45 to 12:10, the energy of longitudinal one was mostly concentrated near 0.5 Hz, but that of the lateral one was near 0.5 Hz or 0.03 Hz. From 12:10 to 14:00, the energy distribution of longitudinal turbulent wind did not change basically except for the sudden change at about 12:25 with the energy transferring to low frequency, which may be due to the decrease of wind speeds.

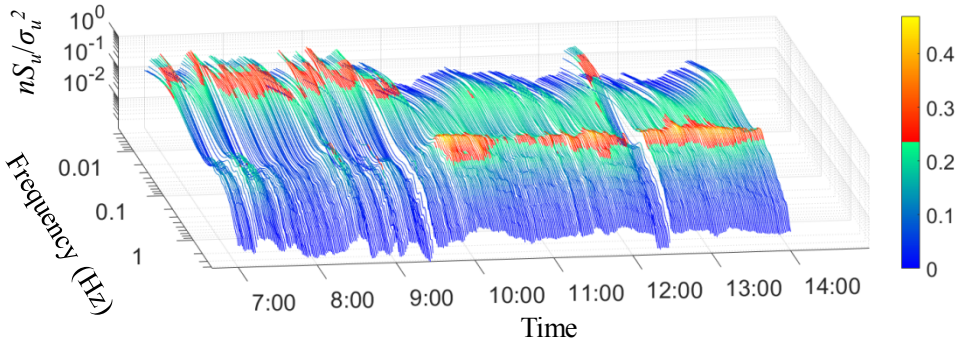

(a)

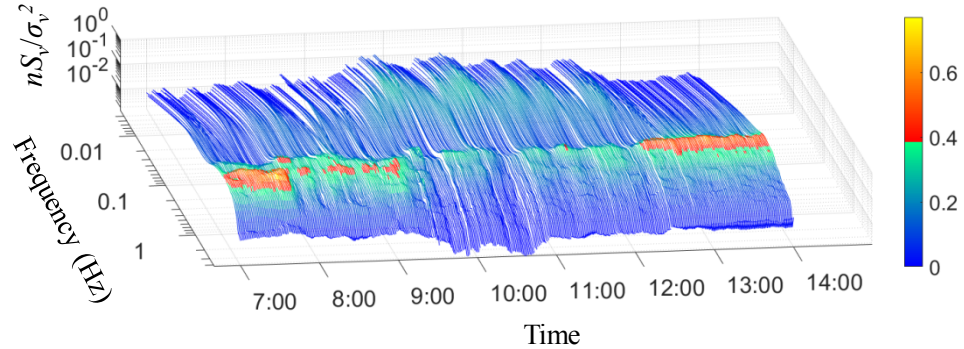

(b)

Fig. 19. Time histories of fluctuation wind power spectrum: (a) longitudinal direction; and (b) lateral direction

According to the assumption of isotropy of turbulent wind, a generalized power spectral density (PSD) was derived in Ref. [21], which is defined as follows.

Longitudinal direction:

$$\frac{nS_u(n)}{\sigma_u^2} = \frac{4f_u}{(1+\mathrm{A}f_u^{\ b})^c} \tag{19}$$

Lateral direction:

$$\frac{nS_v(n)}{\sigma_v^2} = \frac{4f_v(1+B(1+de)f_v^e)}{(1+Bf_v^e)^{d+1}} \tag{20}$$

where A, b, c, B, d, and e = the parameters to be fitted; n = frequency; $f_u = \frac{nL_u^x}{U}$; $f_v = \frac{nL_v^x}{U}$; S_u and S_v = PSDs of the turbulent wind in the longitudinal and lateral directions, respectively; and σ_u and σ_v = the RMSs of the fluctuating component in longitudinal and lateral directions, respectively. According to Kolmogrove's hypothesis [36], $S_u(n) \propto f^{-5/3}$ if $n \to \infty$, thus equation (19) can be modified as:

$$\frac{nS_u(n)}{\sigma_u^2} = \frac{4f_u}{(1+Af_u^b)^{\frac{5}{3b}}} \tag{21}$$

Given A = 70.8, b = 2, B = 283, d = 5/6, and e = 2, equations (24) and (22) become Von Karman spectrum. Data with relatively stable wind characteristics from 10:00 to 13:50 are selected to calculate the spectra and fitted using equations (20) and (21), with the results that A = 5.401, b = 0.982, B = 226.596, d = 0.880, and e =1.761.

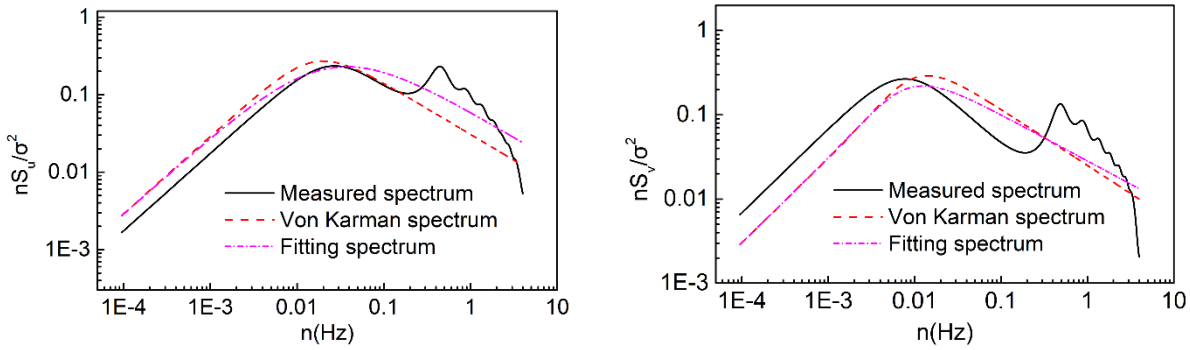

(a) (b)

Fig. 20. Fluctuation wind power spectrum of (a) longitudinal direction; and (b) lateral direction

Fig. 20 shows the comparison between measured, fitting, and Von Karman spectra. The longitudinal Von Karman spectrum is similar to the measured spectrum, and its value is slightly higher than the measured spectrum in the low frequency part. However, there are large differences in the lateral direction spectra, and the Von Karman spectrum is higher than the measured one. Based on the measured spectra, both the two direction spectra have one more peak in high frequency part and the lateral one is more prominent, as indicated in Fig. 20(b). Tamura [36] also found the two peaks phenomenon according to a measured wind speed before and after a typhoon center passed a certain place. It means that the spectrum characteristics of typhoon are different from those of normal wind. Unlike the streamlined bodies, the tall buildings are bluff against the flow, which could cause the flow to separate, rather than to follow body contours [37]. In addition, the disturbance of the wind field caused by the vortex shedding from the building itself may also cause two peaks in spectrum.

5. Conclusions

Based on the measured wind speed and direction atop the Shanghai Tower, the correlations of the mean wind speeds in different averaging times were analyzed using a non-stationary wind velocity model. The fluctuation wind characteristics at evolutional stages of the typhoon including turbulence intensity, gust factor, integral scale of turbulence and power spectrum were discussed and compared with several typhoons measured atop the other super-tall buildings. The relevant conclusions could provide useful information for the high altitude wind features in dense building landform and aid the wind-resistant

design of 600 m+ super-tall buildings. Some conclusions are drawn as follows:

(1) The method of the wavelet hard-threshold denoising, combined with moving window technology, can remove the abnormal value of data effectively, without altering the signal characteristics. However, it should be noted that the data of wind direction need to be "continuously transformed" before applying these preprocessing.

(2) There is a relatively stable ratio between the average wind speeds in 10 min and 1 hour duration time, e.g., $\overline{v}_{1h}$:$\overline{v}_{10min}$ = 0.962 : 1, and both of them can reflect the main change of wind velocity. Since 3 s mean wind speed is sensitive to samples, it is not suitable as duration time.

(3) During the period when the typhoon is stable, the longitudinal and lateral turbulence intensities decrease with the increase of the mean wind speeds, with the linear relationships of I_u = -0.879U + 0.771 and I_v = -0.044U + 0.761. The ratio of longitudinal turbulence intensity to the lateral one is 1:0.835 for most of the time. The turbulence intensities calculated by different measured samples are quite different, so the samples should be selected from the period with stable wind characteristics.

(4) Gust factors decrease with the mean wind speeds, and there exists linear relationships: Gu = -0.982U + 2.752 and Gv = -0.0833U + 1.178. There is a slight difference between the linear and nonlinear fitting of three longitudinal parameters, i.e. the gust factor, turbulence intensity and gust duration time, but obvious error exists as to the linear fitting of the lateral parameters. The nonlinear fitting results are safer for the bearing capacity design of the curtain structures.

(5) The integral scales of turbulence are larger than the horizontal size of the Shanghai Tower during most of the time of the typhoon, indicating that the wind may excite the structure relative violently. In addition, the spectra of turbulent velocity show various characteristics in different stages. Thus, it is necessary to pay attention to the evolution of wind field characteristics when analyzing the measured data of typhoon.

Acknowledgments

The research described in this paper was financially supported by National Natural Science Foundation of China (NSFC) (grant No. 51878475). The financial support is gratefully acknowledged.

References

[1] F.Q. Meng, B.J. He, J. Zhu, D.X. Zhao A. Darko, Z.Q. Zhao, Sensitivity analysis of wind pressure coefficients on CAARC standard tall buildings in CFD simulations, *Journal of Building Engineering*. 16 (2018) 146-158. https://doi.org/10.1016/j.jobe.2018.01.004.

[2] O.J. Andersen, J. Lovseth, Gale force maritime wind. The Frøya data base. Part I: Sites and instrumentation. Review of the data base, *Journal of Wind Engineering and Industrial Aerodynamics*. 57 (1) (1995) 97-109. https://doi.org/10.1016/0167-6105(94)00101-I.

[3] J.A. Wills, A. Grant, C.F. Boyack, Offshore mean wind profile, *Department of Energy, London, Offshore Technology Report*. OTH86-226, 1986. http://hdl.handle.net/10068/619666.

[4] X. Wang, P. Huang, X.F. Yu, X.R. Wang, H.M. Liu, Wind characteristics near the ground during typhoon Meari, *Journal of Zhejiang University-Science A*. 18 (1) (2017) 33-48. https://doi.org/10.1631/jzus.A1500310.

[5] X. Wang, C. Huang, P. Huang, X. Yu, Study on wind characteristics of a strong typhoon in near-ground boundary layer, *Structural Design of Tall and Special Buildings*. 26 (5) (2017). https://doi.org/10.1002/tal.1338.

[6] L. Li, Y. Xiao, H. Zhou, F. Xing, L. Song, Turbulent wind characteristics in typhoon Hagupit based on field measurements, *International Journal of Distributed Sensor Networks*. 14 (10) (2018). https://doi.org/10.1177/1550147718805934.

[7] L.L. Song, Q.S. Li, W.C. Chen, P. Qin, H.H. Huang, Y.C. He, Wind characteristics of a strong typhoon in marine surface boundary layer, *Wind and Structures*. 15 (1) (2012) 1-15.

https://doi.org/10.12989/was.2012.15.1.001.
[8] J.M.W Brownjohn, T.C. Pan, H.K. Cheong, Dynamic response of Republic Plaza, Singapore, *Structural Engineer London*. 76 (11) (1998) 221-226.
[9] Q.S. Li, L.H. Zhi, A.Y. Tuan, C.S. Kao, S.C. Su, C.F. Wu, Dynamic behavior of Taipei 101 Tower: Field measurement and numerical analysis, *Journal of Structural Engineering*. 137 (1) (2011) 143-155. https://doi.org/10.1061/(asce)st.1943-541x.0000264.
[10] T. Kijewski-Correa, D.K. Kwon, A. Kareem, A. Bentz, Y. Guo, S. Bobby, A. Abdelrazaq, SmartSync: An integrated real-time structural health monitoring and structural identification system for tall buildings, *Journal of Structural Engineering*. 139 (10) (2013) 1675-1687. https://doi.org/10.1061/(ASCE)ST.1943-541X.0000560.
[11] J.P. Amezquita-Sanchez, H. Adeli, Signal processing techniques for vibration-based health monitoring of smart structures, *Archives of Computational Methods in Engineering*. 23 (1) (2016) 1-15. https://doi.org/10.1007/s11831-014-9135-7.
[12] T. Liu, B. Yang, Q.L. Zhang, Health monitoring system developed for Tianjin 117 high-rise building, *Journal of Aerospace Engineering*. 30 (2) (2017). https://doi.org/10.1061/(ASCE)AS.1943-5525.0000602.
[13] Q.S. Li, Y.Q. Xiao, J.R. Wu, J.Y. Fu, Z.N. Li, Typhoon effects on super-tall buildings, *Journal of Sound and Vibration*. 313 (3-5) (2008) 581-602. https://doi.org/10.1016/j.jsv.2007.11.059.
[14] Q.S. Li, X. Li, Y. He, J. Yi, Observation of wind fields over different terrains and wind effects on a super-tall building during a severe typhoon and verification of wind tunnel predictions, *Journal of Wind Engineering and Industrial Aerodynamics*. 162 (2017) 73-84. https://doi.org/10.1016/j.jweia.2017.01.008.
[15] X. Li, Q.S. Li. Monitoring structural performance of a supertall building during 14 tropical cyclones, *Journal of Structural Engineering*. 144 (10) (2018) 04018176. https://doi.org/10.1061/(ASCE)ST.1943-541X.0002145.
[16] Q.S. Li, Y.C. He, Y.H. He, K. Zhou, X.L. Han, Monitoring wind effects of a landfall typhoon on a 600 m high skyscraper, *Structure and Infrastructure Engineering*. 15 (1) (2019) 54-71. https://doi.org/10.1080/15732479.2018.1505923.
[17] C.Q. Wang, Z.N. Li, Q.Z. Luo, L. Hu, Z.F. Zhao, J.X. Hu, X.W. Zhang, Wind characteristics investigation on the roofs of three adjacent high-rise buildings in a coastal area during typhoon Meranti, *Applied Sciences-Basel*. 9 (3) (2019). https://doi.org/10.3390/app9030367.
[18] M.D. Powell, S.H. Houston, T.A. Reinhold, Hurricane Andrew's landfall in south Florida. Part I: Standardizing measurements for documentation of surface wind fields, *Weather and Forecasting*. 11 (3) (1996) 304-328. https://doi.org/10.1175/1520-0434(1996)011<0304:HALISF>2.0.CO;2.
[19] Y. An, Y. Quan, M. Gu. Field measurement of wind characteristics of typhoon Muifa on the Shanghai World Financial Center, *International Journal of Distributed Sensor Networks*. (2012). https://doi.org/10.1155/2012/893739.
[20] Y. Quan, S. Wang, M. Gu, J. Kuang, Field measurement of wind speeds and wind-induced responses atop the Shanghai World Financial Center under normal climate conditions, *Mathematical Problems in Engineering*. (2013). http://doi.org/10.1155/2013/902643.
[21] Z.F. Huang. M. Gu, Field measurement of wind characteristics of typhoon Chan-hom on Shanghai World Financial Center, *Journal of Tongji University (Natural Science)*. 44 (8) (2016) 1205-1211. https://doi.org/10.11908/j.issn.0253-374x.2016.08.010.
[22] J. Wu, H.J. Xu, Q.L. Zhang, Dynamic performance evaluation of Shanghai Tower under winds based on full-scale data, *Structural Design of Tall and Special Buildings*. 28 (9) (2019). http://doi.org/10.1002/tal.1611.
[23] Q.S. Li, X. Li, Y.C. He, Monitoring wind characteristics and structural performance of a supertall building during a landfall typhoon, *Journal of Structural Engineering*. 142(11) (2016) 04016097. https://10.1061/(ASCE)ST.1943-541X.0001564.
[24] Q. Zhang, X. Tang, J. Wu, B. Yang, Online automatic structural health assessment of the Shanghai Tower, *Smart Structures and Systems*. 24 (3) (2019) 319-332. https://doi.org/10.12989/sss.2019.24.3.319.
[25] F. Rizzo, F. Ricciardelli, G. Maddaloni, A. Bonati, A. Occhiuzzi. Experimental error analysis of dynamic properties for a reduced-scale high-rise building model and implications on full-scale behavior, *Journal of*

Building Engineering. 28 (2020) 101067. https://doi.org/10.1016/j.jobe.2019.101067.
[26] S.K. Au, F.L. Zhang, P. To, Field observations on modal properties of two tall buildings under strong wind, *Journal of Wind Engineering and Industrial Aerodynamics*, 101 (2012) 12-23. https://doi.org/10.1016/j.jweia.2011.12.002.
[27] F.L. Zhang, H.B. Xiong, W.X. Shi, X. Ou, Structural health monitoring of Shanghai Tower during different stages using a Bayesian approach, *Structural Control and Health Monitoring*. 23 (2016) 1366-1384. https://doi.org/10.1002/stc.1840.
[28] J.Y. Fu, J.R. Wu, A. Xu, Q.S. Li, Y.Q. Xiao, Full-scale measurements of wind effects on Guangzhou West Tower, *Engineering Structures*. 35 (2012) 120-139. https://doi.org/10.1016/j.engstruct.2011.10.022.
[29] K. Wijesooriya, D. Mohotti, K. Chauhan, D. Dias-da-Costa. Numerical investigation of scale resolved turbulence models (LES, ELES and DDES) in the assessment of wind effects on supertall structures, *Journal of Building Engineering*. 25 (2019). https://doi.org/10.1016/j.jobe.2019.100842.
[30] Z.K. Wu, L. Zhao, L.D. Zhu, Y.J. Ge. Hight-altitude observation about turbulence characteristics for "Krose" (0716) strong typhoon, *Acta Aerodynamica Sinica*, 28 (3) (2010) 291-296. https://doi.org/10.3969/j.issn.0258-1825.2010.03.009.
[31] H. Ishizaki, Wind profiles, turbulence intensities and gust factors for design in typhoon-prone regions, *Journal of Wind Engineering & Industrial Aerodynamics*. 13 (1) (1983) 55-66. https://doi.org/10.1016/0167-6105(83)90128-9.
[32] E.C.C. Choi, Gradient height and velocity profile during typhoons, *Journal of Wind Engineering and Industrial Aerodynamics*. 13 (1) (1983) 31-41. https://doi.org/10.1016/0167-6105(83)90126-5.
[33] E. Simiu, R.H. Scanlan. Wind effects on structures. New York: Wiley, 1996.
[34] R.G. Flay, D.C. Stevenson. Integral length scales in strong winds below 20 m, *Journal of Wind Engineering and Industrial Aerodynamics*. 28 (1-3) (1988) 21-30. https://doi.org/10.1016/0167-6105(88)90098-0.
[35] Y.Q. Xiao, J. C. Sun, Q.S. Li, Turbulent integral scale and fluctuation wind speed spectrum of typhoon: an analysis based on field measurements, *Journal of Natural Disasters*. 15 (5) (2006) 45-53. https://doi.org/10.3969/j.issn.1004-4574.2006.05.008.
[36] Y. Tamura, A. Kareem. Advanced structural wind engineering, *Springer*, Japan, 2013. https://doi.org/10.1007/978-4-431-54337-4.
[37] A. Sharma, H. Mittal, A. Gairola, Mitigation of wind load on tall buildings through aerodynamic modifications: Review, *Journal of Building Engineering*. 18 (2018) 180-194. https://doi.org/10.1016/j.jobe.2018.03.005.